Study of K^-p Interactions at 4.1 and 5.5 GeV/c: Final States with Two Charged Particles and a Visible Λ*

J. MOTT,† R. AMMAR, R. DAVIS, W. KROPAC, D. SLATE, AND B. WERNER
Northwestern University, Evanston, Illinois 60201

AND

S. DAGAN,‡ M. DERRICK, T. FIELDS,§ J. LOKEN, AND F. SCHWEINGRUBER
Argonne National Laboratory, Argonne Illinois 60439

(Received 31 July 1968)

The results described in this paper were obtained from an analysis of bubble-chamber pictures of K^-p interactions at incident momenta of 4.1 and 5.5 GeV/c. This paper reports the results on quasi-two-body final states, which are observed to be predominantly peripheral. In the final states $\Lambda\rho$, $\Lambda\omega$, $\Lambda\phi$, and $Y_1^{*+}(1385)\pi^-$, the exchange mechanisms were investigated in terms of the density-matrix formalism. In general, vector-meson exchange appeared to be dominant, and in particular the decay distributions of the $Y_1^{*+}(1385)\pi^-$ final state were in good agreement with the predictions of the Stodolsky-Sakurai model. Several reactions show small backward peaks expected from baryon exchange. The prediction of the independent quark model and other symmetry schemes that the forward cross sections for $\Lambda\rho^0$ and $\Lambda\omega$ production should be equal is well satisfied by the present data. We also report measurements of the properties of various resonant states. We find a mass and width for the $Y_1^*(1695)$ of $M=1700\pm20$ MeV, $\Gamma=130\pm25$ MeV. The dominant decay mode is $\Lambda\pi^+$, but limits are placed on other possible channels.

I. INTRODUCTION

THE data presented here were obtained from an analysis of K^-p interactions at 4.1 and 5.5 GeV/c in the 30-in. hydrogen bubble chamber at Argonne National Laboratory. Neighboring momenta for which final results have been reported are 2.24,[1] 3,[2] 3.5,[3] and 6 GeV/c.[4]

The track configuration scanned for consisted of two prongs with an observed decaying neutral (two-prong $+V$). In this paper we report only on those events in which the neutral particle is a Λ.[5] Table I lists the hypotheses tried on all events in kinematic fitting. The $\Lambda\pi^+\pi^-\gamma$ hypothesis was also tried on a subset of the events as discussed in Sec. VII. Table II gives the two-body final states analyzed in some detail. Results based on some of these have already been reported by this

TABLE I. Hypotheses tried.

$K^-p\to\pi^+\pi^-\Lambda$	$p\bar{p}\Sigma^0$
$\pi^+\pi^-\Lambda\pi^0$	$p\pi^-\Lambda\bar{n}$
$\pi^+\pi^-\Sigma^0$	$\pi^+\bar{p}\Lambda n$
$\pi^+\pi^-\Lambda\eta$	$p\pi^-\bar{K}^0$
$K^+K^-\Lambda$	$p\pi^-\bar{K}^0\pi^0$
$K^+K^-\Lambda\pi^0$	$p\pi^-\bar{K}^0\eta$
$K^+K^-\Sigma^0$	$\pi^+\pi^-\bar{K}^0n$
$K^+K^-\Lambda\eta$	$K^+K^-\bar{K}^0n$
$p\bar{p}\Lambda$	$p\bar{p}\bar{K}^0n$
$p\bar{p}\Lambda\pi^0$	

TABLE II. Two-body final states selected for analysis.

Hypothesis considered	Final state
$\Lambda\pi^+\pi^-$	$\Lambda\rho^0$
	Λf
	$Y_1^{*+}(1385)\pi^-$
	$Y_1^{*+}(1695)\pi^-$
$\Sigma^0\pi^+\pi^-$	$\Sigma^0\rho^0$
	$Y_1^{*+}(1385)\pi^-$
$\Lambda\pi^+\pi^-\pi^0$	$\Lambda\eta$
	$\Lambda\omega$
	$Y_1^{*+,0,-}(1385)\rho^{-,0,+}$
$\Lambda\pi^+\pi^-\eta$	
$\Lambda\pi^+\pi^-\gamma$	ΛX^0
ΛK^+K^-	$\Lambda\phi$
	Λf^*
$\Sigma^0K^+K^-$	$\Sigma^0\phi$
$\Lambda K^+K^-\pi^0$	$Y_1^{*0}(1385)\phi$

* Supported by the National Science Foundation and U. S. Atomic Energy Commission.

† A dissertation based on this work has been submitted to Northwestern University in partial fulfillment of the requirements for the Ph.D. degree.

‡ Now at the University of Tel-Aviv, Tel-Aviv, Israel.

§ Also at Northwestern University, Evanston, Ill.

[1] G. W. London, R. R. Rau, N. P. Samios, S. S. Yamamoto, M. Goldberg, S. Lichtman, M. Primer, and J. Leitner, Phys. Rev. **143**, 1034 (1966).

[2] J. Badier, M. Demoulin, J. Goldberg, B. P. Gregory, P. Krejbich, C. Pelletier, M. Ville, R. Barloutaud, A. Levèque, C. Louedec, J. Meyer, P. Schlein, A. Verglas, E. S. Gelsema, J. Hoogland, J. C. Kluyver, and A. G. Tenner, in *Proceedings of the Twelfth International Conference on High-Energy Physics, Dubna, 1964* (Atomizdat, Moscow, 1966), Vol. 1, p. 650.

[3] N. Haque, R. Scotter, B. Musgrave, W. M. Blair, A. L. Grant, I. S. Hughes, P. J. Negus, R. H. Turnbull, A. A. Z. Ahmed, S. Baker, L. Celnikier, S. Misbahuddin, H. J. Sherman, I. O. Skillicorn, A. R. Atherton, A. D. Brody, G. B. Chadwick, W. T. Davies, J. H. Field, P. M. D. Gray, D. E. Lawrence, J. G. Loken, L. Lyons, J. H. Mulvey, A. J. Oxley, C. A. Wilkinson, C. M. Fisher, E. Pickup, L. K. Rangan, J. M. Scarr, and A. M. Segar, Phys. Rev. **152**, 1148 (1966).

[4] D. C. Colley, W. P. Dodd, F. Macdonald, B. Musgrave, S. K. Tuli, W. Blair, R. Erskine, J. Gordon, I. Hughes, R. Turnbull, P. Chaudhuri, A. Eskreys, S. J. Goldsack, K. Paler, K. Sisterson, W. Blum, G. Dehm, N. Schmitz, W. Schrankel, J. Allison, W. W. M. Allison, A. D. Brody, D. H. Locke, L. Lyons, P. Finney, C. Fischer, L. K. Rangan, and A. Segar, Nuovo Cimento **53A**, 522 (1968).

[5] Results from events in which the neutral particle is a $\bar{K}^0$ have been previously reported; see F. Schweingruber, M. Derrick, T. Fields, D. Griffiths, L. G. Hyman, R. J. Jabbur, J. Loken, R. Ammar, R. E. P. Davis, W. Kropac, and J. Mott, Phys. Rev. **166**, 1317 (1968).

collaboration,[6–8] but a reanalysis is presented whenever a larger amount of data is available.

The basic purposes of the experiment were fourfold: to search for new particles, to determine the quantum numbers of new particles, to investigate the production mechanisms of all resonances produced with a sufficiently large signal, and finally to compare the results on two-body final states with the predictions of various theoretical models.

The production mechanisms were investigated by analyzing the production angular distributions of the two-body final states together with decay correlations of the resonances and comparing the results with

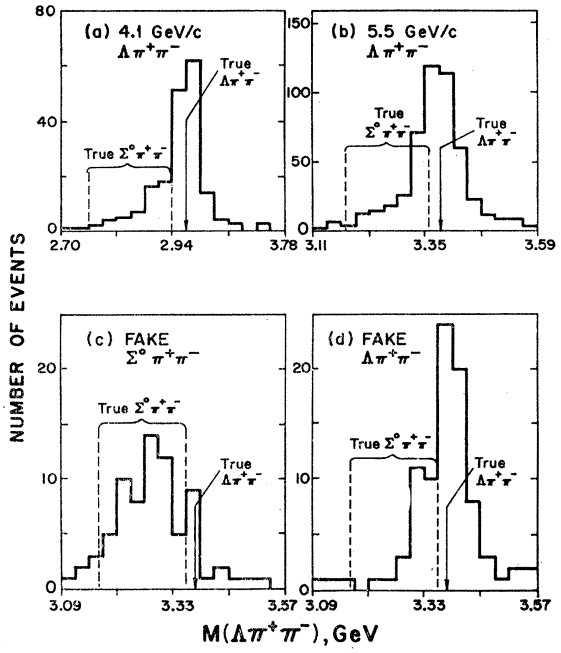

FIG. 1. The unfitted $\Lambda\pi^+\pi^-$ mass distributions. (a) Experimental $\Lambda\pi^+\pi^-$ fits at 4.1 GeV/c. Without measurement errors, true $\Lambda\pi^+\pi^-$ events have a $\Lambda\pi^+\pi^-$ mass of 2.973 GeV while true $\Sigma^0\pi^+\pi^-$ events range from 2.79 to 2.95 GeV. (b) Experimental $\Lambda\pi^+\pi^-$ fits at 5.5 GeV/c. Without measurement errors, true $\Lambda\pi^+\pi^-$ events have a $\Lambda\pi^+\pi^-$ mass of 3.386 GeV while $\Sigma^0\pi^+\pi^-$ events range from 3.17 to 3.36 GeV. (c) $\Sigma^0\pi^+\pi^-$ events generated by FAKE at 5.5 GeV/c. (d) $\Lambda\pi^+\pi^-$ events generated by FAKE at 5.5 GeV/c.

theoretical models. For the two-body production of hyperon resonances, the model of Stodolsky and Sakurai[9] of vector exchange with $M1$ dominance makes specific predictions for the density matrix elements which are compared with the data of this experiment.

[6] J. Mott, R. Ammar, R. E. P. Davis, W. Kropac, F. Schweingruber, M. Derrick, T. Fields, L. G. Hyman, J. Loken, and J. Simpson, Phys. Rev. Letters **18**, 355 (1967).

[7] M. Derrick, T. Fields, J. Loken, R. Ammar, R. E. P. Davis, W. Kropac, J. Mott, and F. Schweingruber, Phys. Rev. Letters **18**, 266 (1967).

[8] R. Ammar, R. E. P. Davis, C. Hwang, W. Kropac, J. Mott, B. Werner, S. Dagan, M. Derrick, F. Schweingruber, and J. Simpson, Phys. Rev. Letters **19**, 1071 (1967).

[9] L. Stodolsky and J. J. Sakurai, Phys. Rev. Letters **11**, 90 (1963); Leo Stodolsky, Phys. Rev. **134**, B1099 (1964).

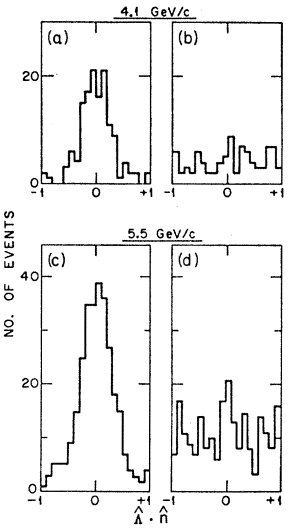

FIG. 2. A histogram of the quantity $\cos\theta=\hat{\Lambda}\cdot\hat{n}$, where $\hat{n}$ is the unit normal to the Σ^0 production plane and $\hat{\Lambda}$ is the unit vector in the direction of the Λ in the Σ^0 c.m. system. For real $\Lambda\pi^+\pi^-$ events, $\hat{n}$ is essentially normal to $\hat{\Lambda}$, so that one expects a distribution peaked at $\cos\theta=0$. (a) The $(\Lambda/\Sigma^0)\pi^+\pi^-$ ambiguities at 4.1 GeV/c. (b) All $\Sigma^0\pi^+\pi^-$ fits at 4.1 GeV/c which are not ambiguous with $\Lambda\pi^+\pi^-$. (c) and (d) are corresponding histograms at 5.5 GeV/c.

Finally, the independent-quark model[10] makes specific predictions for several two-body final states which are observed in the present experiment.[6]

II. EXPERIMENTAL DETAILS

A. Exposure and Analysis

We analyzed 90 000 pictures at 4.1 GeV/c and 400 000 pictures at 5.5 GeV/c, representing 3.6×10^7 cm and

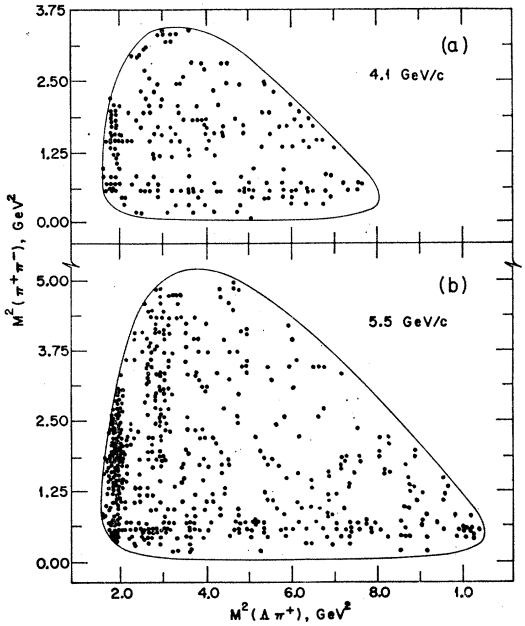

FIG. 3. Dalitz plots for 213 $\Lambda\pi^+\pi^-$ events at 4.1 GeV/c, and 563 events at 5.5 GeV/c.

[10] G. Alexander, H. J. Lipkin, and F. Scheck, Phys. Rev. Letters **17**, 412 (1966); H. J. Lipkin and F. Scheck, *ibid.* **16**, 71 (1966); E. M. Levin and L. L. Frankfurt, JETP Pis'ma v Redaktsiyu **2**, 105 (1965) [English transl.: JETP Letters **2**, 65 (1965)].

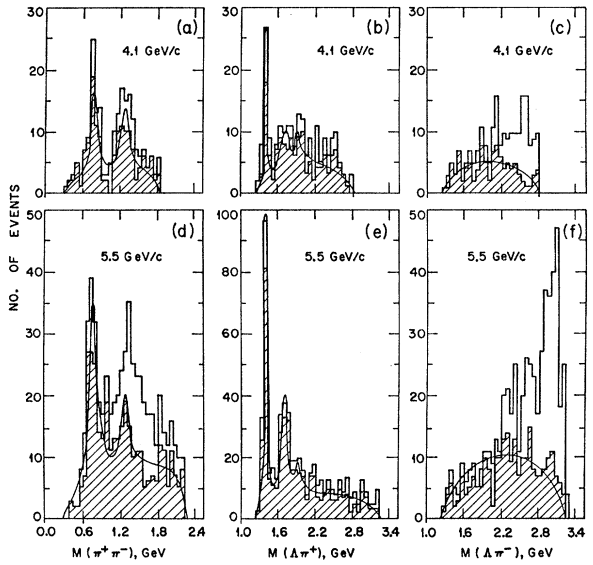

FIG. 4. Mass projections for the $\Lambda\pi^+\pi^-$ final state. In making fits to the Breit-Wigner resonance shape, the mass and width used for each resonance was that which gave a best fit to the combined data at 4.1 and 5.5 GeV/c. (a) The $\pi^+\pi^-$ mass at 4.1 GeV/c. The shaded area contains 149 events after subtraction of 64 $Y_1^{*+}(1385)\pi^-$ and $Y_1^{*+}(1695)\pi^-$ events. The solid curve is a best fit to the shaded histogram for phase space and two Breit-Wigner resonances with $M(\rho^0)=755$ MeV, $\Gamma(\rho^0)=140$ MeV, and $M(f)=1285$ MeV, $\Gamma(f)=140$ MeV. The relative contributions are 49% phase space, 29% ρ^0 and 22% f. (b) The $\Lambda\pi^+$ mass at 4.1 GeV/c. The shaded area contains 144 events after subtraction of 69 $\Lambda\rho^0$ and Λf events. The solid curve is a best fit to the shaded histogram for phase space and three Breit-Wigner resonances with $M(Y_1^{*+}(1385))=1383$ MeV, $\Gamma(Y_1^{*+}(1385))=31$ MeV, $M(Y_1^{*+}(1695))=1700$ MeV, $\Gamma(Y_1^{*+}(1695))=130$ MeV, and $M(Y_1^{*}(1910))=1910$ MeV, $\Gamma(Y_1^{*+}(1910))=60$ MeV. The relative contributions are 67% phase space, 14% $Y_1^{*+}(1385)$, 15% $Y_1^{*+}(1695)$, and 4% $Y_1^{*+}(1910)$. (c) The $\Lambda\pi^-$ mass at 4.1 GeV/c. The shaded area contains 101 events after subtraction of 112 $\Lambda\rho^0$, Λf, $Y_1^{*+}(1385)\pi^-$, and $Y_1^{*+}(1695)\pi^-$ events. The solid curve is phase-space normalized to the shaded histogram. (d) The $\pi^+\pi^-$ mass at 5.5 GeV/c. The shaded area contains 345 events after subtraction of 218 $Y_1^{*+}(1385)\pi^-$ events and $Y_1^{*+}(1695)\pi^-$ events. The solid curve is a best fit to the shaded histogram for phase space and the two Breit-Wigner resonances described in (a). The relative contributions are 60% phase space, 30% ρ^0, and 10% f. (e) The $\Lambda\pi^+$ mass at 5.5 GeV/c. The shaded area contains 432 events after subtraction of 131 $\Lambda\rho^0$ and Λf events. The solid curve is a best fit to the shaded histogram for phase space and the three Breit-Wigner resonances described in (b). The relative contributions are 45% phase space, 28% $Y_1^{*+}(1385)$, 25% $Y_1^{*+}(1695)$, and 2% $Y_1^{*+}(1910)$. (f) The $\Lambda\pi^-$ mass at 5.5 GeV/c. The shaded area contains 248 events after subtraction of 315 $\Lambda\rho^0$, Λf, $Y_1^{*+}(1385)\pi^-$, and $Y_1^{*+}(1695)\pi^-$ events. The solid curve is phase-space normalized to the shaded area.

2.22×10^8 cm of K^- track, respectively. The separated K^- beam[11] from the Zero Gradient Synchrotron (ZGS) was of high purity, having $\sim10\%$ contamination of light particles at 4.1 GeV/c and $\sim5\%$ at 5.5 GeV/c.

[11] T. H. Fields, E. L. Goldwasser, and U. E. Kruse, Argonne National Laboratory Report No. THF/ELG/UEK-1, 1961 (unpublished). R. Ammar, T. H. Fields, M. Derrick, E. L. Goldwasser, M. L. Good, U. E. Kruse, D. Reeder, F. Schweingruber, and J. D. Simpson, in Proceedings of 1966 International Conference on Instrumentation for High-Energy Physics, Stanford USAEC Conf. 660918 (International Union of Pure and Applied Physics and U. S. Atomic Energy Commission, Washington, D. C., 1966), p. 620.

At the scanning stage, ionization estimates were made for all tracks. This information and measurement data from the digitized projectors were analyzed by a system of computer programs (MASMER, HGEOM, GRIND, SUMTAP, SUMEDIT, and SUMX), which performed the necessary bookkeeping, reconstruction, kinematic fitting, and plotting of histograms. Details on these programs as well as further details on the exposure may be found in Ref. 5.

Events were considered ambiguous if they fit more than one of the complete set of hypotheses listed in Table I. Hypotheses containing an unobserved Λ or $\bar{K}^0$ have not been considered since they are expected to have few events.

Kinematic ambiguities were investigated by using such auxiliary information as ionization, mass plots calculated from the unfitted kinematical values, and properties of events generated artificially by FAKE.[12] Detailed treatment of such ambiguities will be discussed for the individual final states.

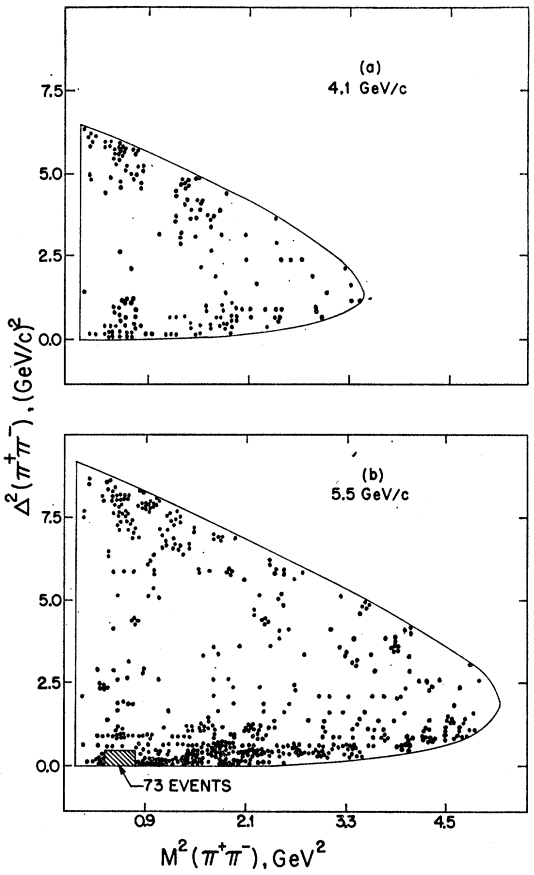

FIG. 5. Chew-Low plots for the $\pi^+\pi^-$ system in the $\Lambda\pi^+\pi^-$ events. The events have been weighted as described in Sec. II B.

[12] G. R. Lynch, University of California Radiation Laboratory Report No. UCRL-10335, 1966 (unpublished).

B. Cross-Section Basis

To determine the K^- flux, a beam count was done every 20 frames. In addition, three-prong events were recorded in the regular scanning. The incident K^- flux calculated from the known three-prong branching ratio of K^- decay[13] was in agreement with that derived from the beam count and the beam purity which was measured by a Čerenkov counter during the exposure.

The combined scan efficiency was 99% as determined from two complete scans of the film. Events found in the first scan which had failed the computer programs were remeasured along with the new events found in the second scan. Of the total number of events, 5% finally failed to give a satisfactory geometrical reconstruction.

In the course of testing the kinematic fitting program with artificially generated events, it was found that (30±10)% of Σ^0 events did not yield a satisfactory fit. This loss was taken into account in the Σ^0 cross-section estimate.

For absolute cross-section measurements and angular distributions, the events were restricted to within a fiducial volume which was slightly smaller than the scanned volume. Both the primary and V vertices had to lie within a restricted volume and in addition the Λ was required to have a flight path length greater than 0.5 cm. Using the known Λ lifetime,[13] each observed event was then weighted to correct for Λ particles decaying outside the fiducial volume or within 0.5 cm

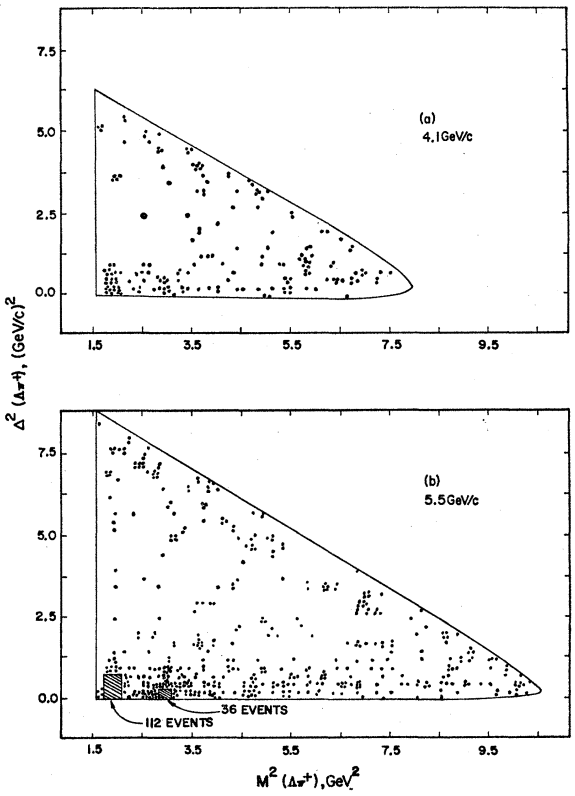

FIG. 6. Chew-Low plots for the $\Lambda\pi^+$ system in the $\Lambda\pi^+\pi^-$ events. The events have been weighted as described in Sec. II B.

TABLE III. Cross sections derived from $\Lambda\pi^+\pi^-$ and $\Sigma^0\pi^+\pi^-$ events.

Reaction channel	Total No. of events 4.1 GeV/c	Total No. of events 5.5 GeV/c	Weighted No. of events[a] 4.1 GeV/c	Weighted No. of events[a] 5.5 GeV/c	σ (μb) for decay into particles observed 4.1 GeV/c	σ (μb) for decay into particles observed 5.5 GeV/c	σ (μb) corrected for other decay modes (Ref. 13) 4.1 GeV/c	σ (μb) corrected for other decay modes (Ref. 13) 5.5 GeV/c
$\Lambda\pi^+\pi^-$	213±15	563±25	186±18	652±30	305±53	135±12		
$\Lambda\rho^0$	45±11	107±13	40±13	105±15	66±23	22± 4	66±23	22± 4
$\rightarrow\pi^+\pi^-$								
Λf	35±10	39±10	32±13	38±12	53±22	8± 3	80±33	12± 5
$\rightarrow\pi^+\pi^-$								
$Y_1^{*+}(1385)\pi^-$	22± 8	129±12	20±8	140±14	33±11	29± 4	36±21	32± 4
$\rightarrow\Lambda\pi^+$								
$Y_1^{*+}(1695)\pi^-$	23±12	112±13	20±16	122±15	33±27	25± 5		
$\rightarrow\Lambda\pi^+$								
$Y_1^{*+}(1910)\pi^-$	6± 6	9± 9	6± 6	10±10	15±15	2± 2		
$\rightarrow\Lambda\pi^+$								
$\Sigma^0\pi^+\pi^-$	41±13	135±20	60±30	150±25	100±50	31± 6		
$\Sigma^0\rho^0$	<4	14± 5	<4	14± 5	<8	3± 1	<8	3±1
$\rightarrow\pi^+\pi^-$								
$Y_1^{*+}(1385)\pi^-$	<4	11± 4	<4	11± 4	<8	2± 1		
$\rightarrow\Sigma^0\pi^+$								

[a] Calculated as described in Sec. II B, using events from a restricted fiducial volume containing ~20% less events than the observed total of the previous column.

[13] A. H. Rosenfeld, N. Barash-Schmidt, A. Barbaro-Galtieri, L. R. Price, Paul Söding, C. G. Wohl, Matts Roos, and W. J. Willis, Rev. Mod. Phys. **40**, 77 (1968).

of the primary vertex. All of the angular distributions in this paper have been so weighted. The average weighting factor was ~1.25. The following cross section bases were found:

$$0.61\pm0.08 \text{ events}/\mu\text{b at } 4.1 \text{ GeV}/c,$$
$$4.85\pm0.30 \text{ events}/\mu\text{b at } 5.5 \text{ GeV}/c,$$

where these numbers include corrections for beam purity, scan efficiency, geometry failures, and neutral decays of the Λ. These cross-section numbers are to be applied to the weighted number of events calculated as described above. Some final states (e.g., $\Lambda\phi$), also require correction for decays of the meson system which do not yield the two-prong+V topology. Such corrections depend on the particular final state and are discussed later.

For the mass histograms, all the events found were used with no fiducial volume selection and with no weighting factor applied.

III. KINEMATIC FITS TO THE $\Lambda\pi^+\pi^-$ HYPOTHESIS

A. Resolution of Ambiguities

There were 213 $\Lambda\pi^+\pi^-$ fits at 4.1 GeV/c and 563 at 5.5 GeV/c, of which ~40% were unique. The ambiguities were almost entirely with the $\Sigma^0\pi^+\pi^-$ final state and were resolved by the methods described below.

The Λ momentum was calculated using the constraint that the V point to the K^-p interaction vertex. This momentum was used along with unfitted momenta of the tracks at the production vertex to calculate the $\Lambda\pi^+\pi^-$ invariant mass $M(\Lambda\pi\pi)$. This should equal the invariant mass of the initial K^-p system for true $\Lambda\pi^+\pi^-$ events and should be lower for true $\Sigma^0\pi^+\pi^-$ events because of the energy carried off by the γ. This expectation, modified by the experimental errors, was verified by an examination of artificial $\Lambda\pi^+\pi^-$ and $\Sigma^0\pi^+\pi^-$ events at 5.5 GeV/c generated by the computer program FAKE.[12] The hypotheses listed in Table I were tried on the artificial events. Figure 1 shows a comparison of $M(\Lambda\pi\pi)$ for the observed $\Lambda\pi^+\pi^-$ fits with that for the FAKE events. The distribution of $M(\Lambda\pi\pi)$ for the observed $\Lambda\pi^+\pi^-$ fits does not show an excess of events in the region expected for $\Sigma^0\pi^+\pi^-$ events, thus indicating that the Σ^0 contamination is not significant.

In addition, the FAKE results indicate that only 35% of the events generated as $\Sigma^0\pi^+\pi^-$ would fit the $\Lambda\pi^+\pi^-$ hypothesis but that 70% of the events generated either as $\Lambda\pi^+\pi^-$ or as $Y_1^{*+}(1385)\pi^-$ would fit the $\Sigma^0\pi^+\pi^-$ hypothesis. This further supports the conclusion that the observed events are mainly $\Lambda\pi^+\pi^-$ (four-constraint fit) rather than $\Sigma^0\pi^+\pi^-$ (two-constraint fit).

Further, since $Y_1^{*+}(1385)$ decays predominantly into $\Lambda\pi^+$ but has only a small decay rate into $\Sigma^0\pi^+$,[13] the amount of the $Y_1^{*+}(1385)$ in the ambiguous events is a measure of the amount of the $\Lambda\pi^+\pi^-$ final state. Experimentally, the fraction of $Y_1^{*+}(1385)$ in the ambiguous events was consistent with interpreting them as predominantly $\Lambda\pi^+\pi^-$ events.

Additional evidence against the interpretation that the $(\Lambda/\Sigma^0)\pi^+\pi^-$ ambiguities represent real $\Sigma^0\pi^+\pi^-$ events arises from an observation of the decay angular distribution of the hypothesized Σ^0. Figure 2 shows a

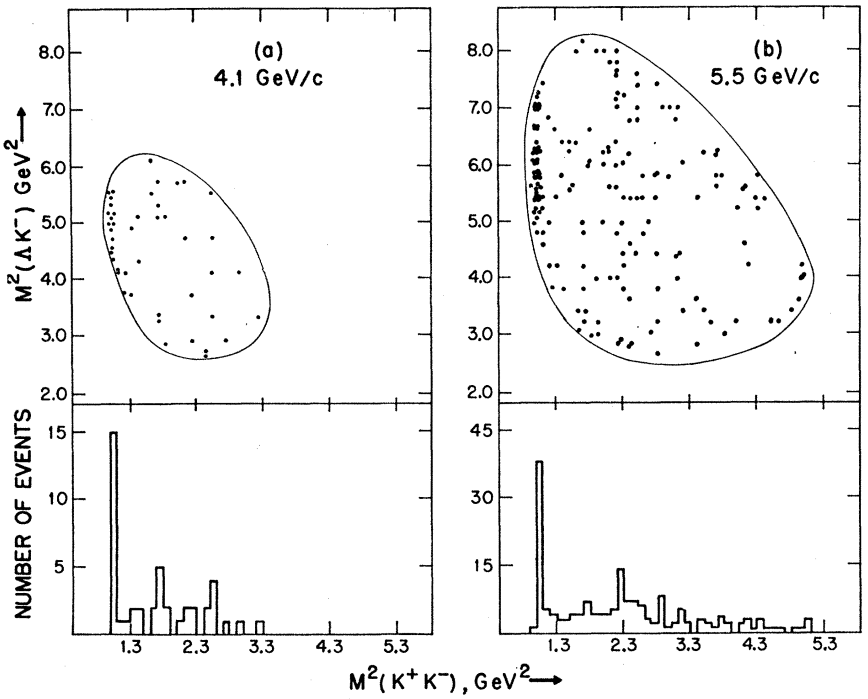

FIG. 7. Dalitz plots and $M^2(K^+K^-)$ projections for 44 ΛK^+K^- events at 4.1 GeV/c and 172 events at 5.5 GeV/c.

histogram of the quantity $\cos\theta=\hat{\Lambda}\cdot\hat{n}$, where $\hat{n}$ is the unit normal to the Σ^0 production plane and $\hat{\Lambda}$ is the unit vector in the direction of the Λ in the Σ^0 c.m. system. For real $\Lambda\pi^+\pi^-$ events, $\hat{n}$ is essentially normal to $\hat{\Lambda}$ so that one expects a distribution peaked at $\cos\theta=0$. The $(\Lambda/\Sigma^0)\pi^+\pi^-$ ambiguities show such a peak while those events which are not ambiguous with the $\Lambda\pi^+\pi^-$ hypothesis, and therefore presumed to be mainly $\Sigma^0\pi^+\pi^-$ events, have an isotropic distribution as expected since the Λ polarization is consistent with being zero. This indicates that the $(\Lambda/\Sigma^0)\pi^+\pi^-$ events belong to a different population than $\Sigma^0\pi^+\pi^-$ events and are consistent with being $\Lambda\pi^+\pi^-$.

On the basis of the preceding analyses, all of the $(\Lambda/\Sigma^0)\pi^+\pi^-$ ambiguities were taken to be $\Lambda\pi^+\pi^-$ events, with a contamination from $\Sigma^0\pi^+\pi^-$ estimated to be about 5%.

B. Display of Data for Two-Body Final States

Dalitz plots of the $\Lambda\pi^+\pi^-$ events at 4.1 and 5.5 GeV/c are shown in Fig. 3, and effective-mass distributions at each momentum are presented in Fig. 4. Evidence for the two-body final states $\Lambda\rho^0$, Λf, and $Y_1^{*+}(1385)\pi^-$ is seen at both momenta. In addition, there is evidence for $Y_1^{*+}(1695)\pi^-$ at 5.5 GeV/c.[7] The f is more evident after subtraction of events in both Y_1^{*+} regions. We also note that production of $Y_1^{*-}(1385)\pi^+$ seems to be absent, and will discuss this later. The production angular distributions as a function of mass are shown in the Chew-Low plots of Figs. 5 and 6.

Cross sections, estimated by fitting the appropriate Breit-Wigner and phase-space contributions in each mass projection, are given in Table III.

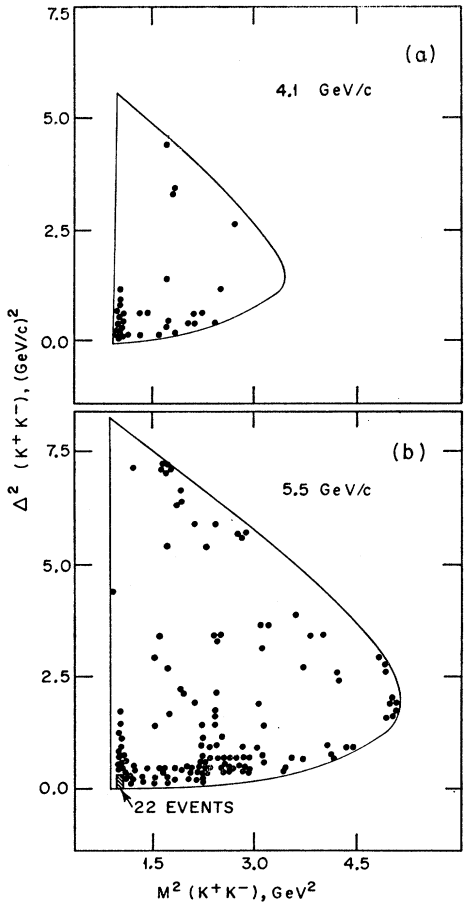

FIG. 8. Chew-Low plots for the K^+K^- system in the ΛK^+K^- events. The events have been weighted as described in Sec. II B.

IV. KINEMATIC FITS TO THE ΛK^+K^- HYPOTHESIS: $\Lambda\phi$ AND Λf^* FINAL STATES

Approximately 95% of the events fitting the ΛK^+K^- hypothesis also fit the $\Sigma^0K^+K^-$ and/or $\Lambda\pi^+\pi^-\pi^0$ hypotheses. The $(\Lambda/\Sigma^0)K^+K^-$ ambiguities were resolved in a manner similar to that used for the $(\Lambda/\Sigma^0)\pi^+\pi^-$ ambiguities, with the conclusion that the events as a whole represented ΛK^+K^- rather than $\Sigma^0K^+K^-$. This procedure also yielded the same conclusion when

TABLE IV. Cross sections derived from the ΛK^+K^- and $\Sigma^0K^+K^-$ final states.

Reaction channel	Total No. of events 4.1 GeV/c	Total No. of events 5.5 GeV/c	Weighted No. of events[a] 4.1 GeV/c	Weighted No. of events[a] 5.5 GeV/c	σ (μb) for decay into particles observed 4.1 GeV/c	σ (μb) for decay into particles observed 5.5 GeV/c	σ (μb) corrected for other decay modes (Ref. 13) 4.1 GeV/c	σ (μb) corrected for other decay modes (Ref. 13) 5.5 GeV/c
ΛK^+K^-	44± 7	172±14	36± 7	170±16	59±13	35± 5		
$\Lambda\phi$, $\phi\to K^+K^-$	14±14	37± 7	13± 4	33± 8	21± 7	7± 2	43±15	14± 4
Λf^*, $f^*\to K^+K^-$	5± 3	36± 8	5± 3	34±10	8± 5	7± 2		
$\Sigma^0K^+K^-$	8± 5	35± 8	8± 5	35±10	13± 8	7± 2		
$\Sigma^0\phi$, $\phi\to K^+K^-$	5± 3	8± 4	5± 3	6± 4	8± 5	1± 1	17±11	2± 2

[a] Calculated as described in Sec. II B, using events from a restricted fiducial volume containing ~20% less events than the observed total of the previous column.

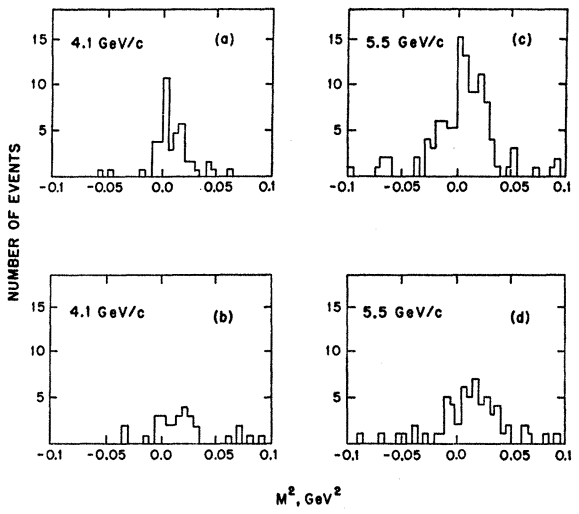

FIG. 9. Histograms of M^2 defined in $K^-+p\rightarrow\Lambda+\pi^++\pi^-+M$. (a) The $\Sigma^0\pi^+\pi^-$ candidates at 4.1 GeV/c after removal of four-constraint fits. (b) $\Lambda\omega$ events at 4.1 GeV/c. (c) and (d) are corresponding plots at 5.5 GeV/c.

applied to smaller subsets of data such as in the $\Lambda\phi$ and Λf^* regions.

The fitted K^+K^- invariant-mass distributions and Dalitz plots of Fig. 7 show ϕ and f^* peaks. Ambiguities between the ΛK^+K^- and $\Lambda\pi^+\pi^-\pi^0$ hypotheses in the ϕ and f^* peaks were resolved by the following considerations. Since the f^* has $G=+1$, it cannot decay strongly into 3π and we can disregard the $\Lambda\pi^+\pi^-\pi^0$ ambiguities in the f^* peak. The ϕ, on the other hand, does have a 3π decay mode but on the basis of the known branching ratios[13] one expects only ~ 6 $\Lambda\phi$ events with a visible Λ and the ϕ decaying into $\pi^+\pi^-\pi^0$, and only a very small fraction of these are expected to contaminate the four-constraint fits. Thus the events in both the ϕ and f^* regions were assigned to the four-constraint fit ΛK^+K^- rather than the one-constraint fit $\Lambda\pi^+\pi^-\pi^0$. The production angular distribution as a function of the K^+K^- mass is shown in Fig. 8. Cross sections derived from the ΛK^+K^- events are shown in Table IV. Properties of the f^* as measured in this experiment have been previously presented[8] and are summarized in Sec. IX E.

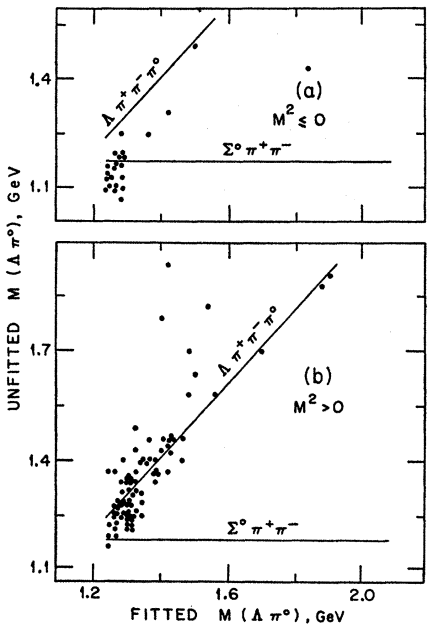

FIG. 10. The unfitted $\Lambda\pi^0$ mass versus the fitted $\Lambda\pi^0$ mass for all the $\Sigma^0\pi^+\pi^-/\Lambda\pi^+\pi^-\pi^0$ ambiguities after removal of events with four-constraint fits at 5.5 GeV/c. (a) Events with $M^2\leq 0$ where M is defined in $K^-+p\rightarrow\Lambda+\pi^++\pi^-+M$. (b) Events with $M^2>0$.

V. KINEMATIC FITS TO THE $\Sigma^0\pi^+\pi^-$ AND $\Sigma^0K^+K^-$ HYPOTHESES

The $\Sigma^0\pi^+\pi^-$ fits which were not ambiguous with the $\Lambda\pi^+\pi^-$ hypothesis were investigated by means of the missing mass M, defined in $K^-+p\rightarrow\Lambda+\pi^++\pi^-+M$. By requiring M to be consistent with a γ rather than with a π^0, we obtain a sample of events which are most likely $\Sigma^0\pi^+\pi^-$. In Fig. 9 we see a histogram of M^2 for $\Sigma^0\pi^+\pi^-$ candidates and for known $\Lambda\omega$ events. One can see that about half of the candidates are likely to be $\Sigma^0\pi^+\pi^-$ events. This method of identifying $\Sigma^0\pi^+\pi^-$ fits gave a fairly clean resolution of the $\Sigma^0\pi^+\pi^-/\Lambda\pi^+\pi^-\pi^0$ ambiguity as seen in Fig. 10, where the fitted $\Lambda\pi^0$ mass is shown as a function of the unfitted mass recoiling from the $\pi^+\pi^-$ system. True $\Lambda\pi^+\pi^-\pi^0$ events lie about the diagonal line where the fitted and unfitted masses are equal, while true $\Sigma^0\pi^+\pi^-$ events should lie along the horizontal line at the Σ^0 mass. Selecting on $M^2>0$, as in Fig. 10(b), one finds that the events are distributed along the diagonal line while selecting on $M^2\leq 0$ yields events most consistent with the $\Sigma^0\pi^+\pi^-$ hypothesis as shown in Fig. 10(a).

Similar results were also found for the $\Sigma^0K^+K^-$ fits. The final definition of $\Sigma^0K^+K^-$ events was that they not be ambiguous with either the $\Lambda\pi^+\pi^-$ or ΛK^+K^- hypotheses and that they have an analogously defined missing mass $M^2\leq 0$. The Σ^0 events thus selected show small amounts of ρ^0, $Y_1^{*+}(1385)$, and ϕ production as seen in Fig. 11. Cross sections derived from these plots were increased by 20% to account for events with $M^2>0$ and 30% to account for the difficulty in kinematic fitting of Σ^0 hypotheses, and are given in Tables III and IV.

VI. KINEMATIC FITS TO THE $\Lambda\pi^+\pi^-\pi^0$ HYPOTHESIS

A. Resolution of Ambiguities

There were 810 fits to the $\Lambda\pi^+\pi^-\pi^0$ hypothesis at 4.1 GeV/c of which 65% were unique, and 2711 fits at 5.5 GeV/c of which 45% were unique. The major ambiguities were with the $\Lambda\pi^+\pi^-\eta$ and $\Lambda K^+K^-\pi^0$ final states. In addition multi-π^0 final states contaminate the sample as discussed below. Events were removed from the above sample if they fit the $\Lambda\pi^+\pi^-$ or ΛK^+K^-

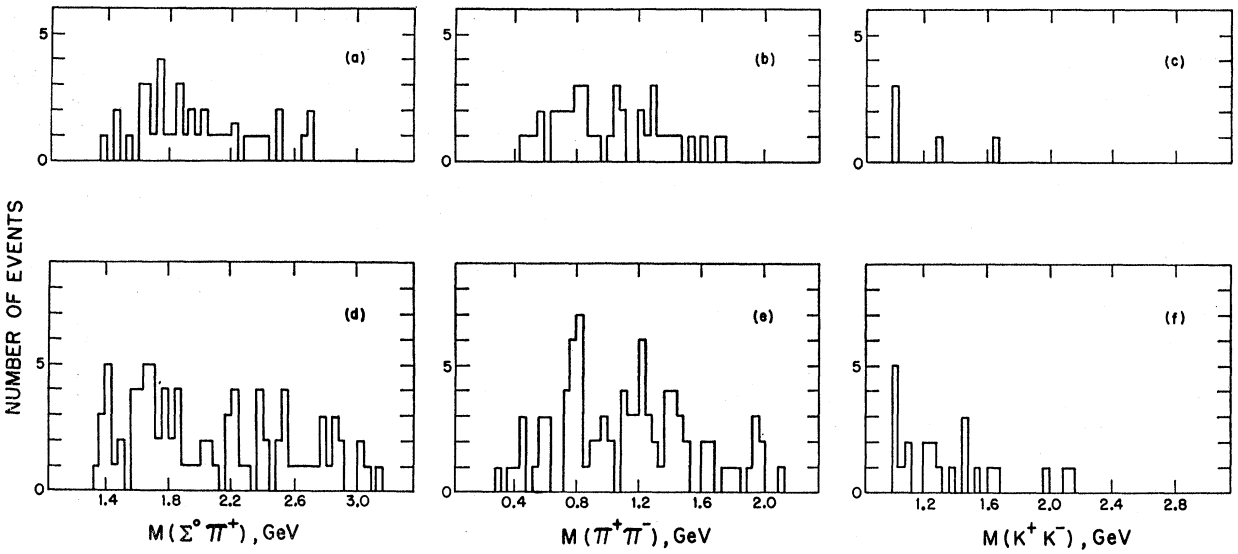

FIG. 11. Mass histograms for a selection of $\Sigma^0\pi^+\pi^-$ fits with $M^2<0$, as defined in $K^-+p\rightarrow\Lambda+\pi^++\pi^-+M$, after removal of events with four-constraint fits, as well as for a corresponding selection of $\Sigma^0K^+K^-$ fits. (a) The $\Sigma^0\pi^+$ mass for 41 $\Sigma^0\pi^+\pi^-$ events at 4.1 GeV/c. (b) The $\pi^+\pi^-$ mass for 41 $\Sigma^0\pi^+\pi^-$ events at 4.1 GeV/c. (c) The K^+K^- mass for 5 $\Sigma^0K^+K^-$ events at 4.1 GeV/c. (d) The $\Sigma^0\pi^+$ mass for 89 $\Sigma^0\pi^+\pi^-$ events at 5.5 GeV/c. (e) The $\pi^+\pi^-$ mass for 89 $\Sigma^0\pi^+\pi^-$ events at 5.5 GeV/c. (f) The K^+K^- mass for 23 $\Sigma^0K^+K^-$ events at 5.5 GeV/c.

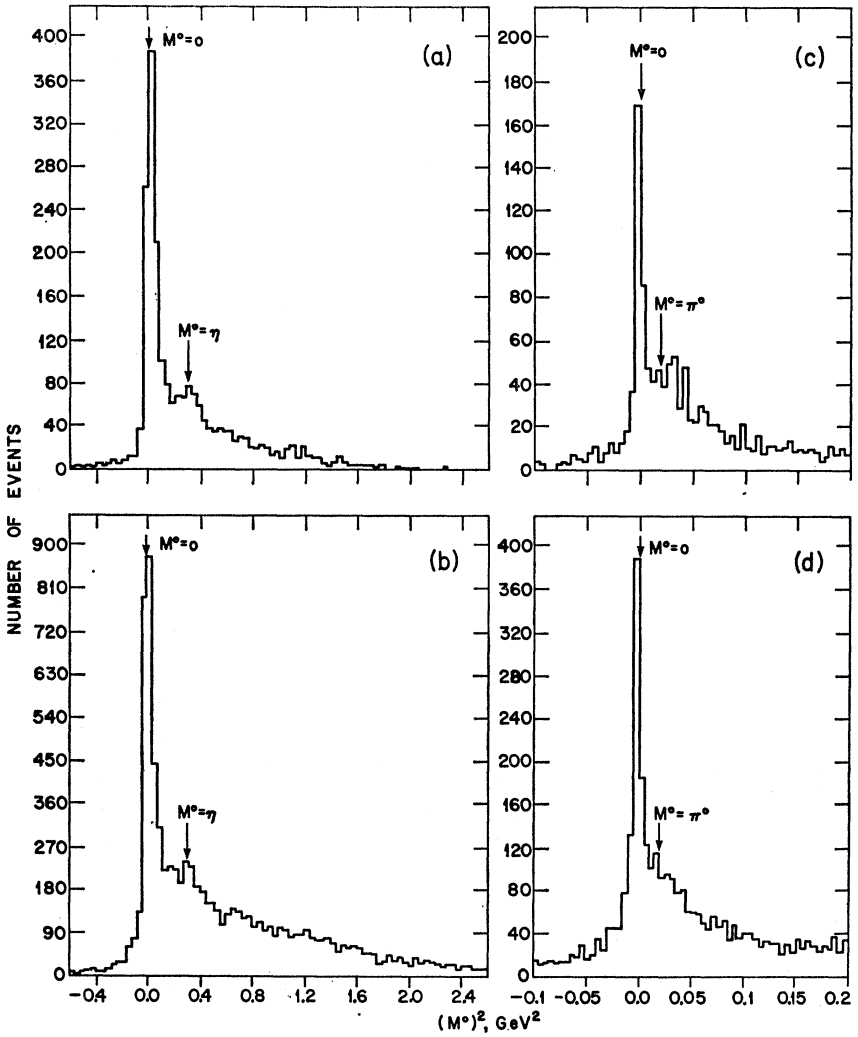

FIG. 12. Distribution of the square of the mass M^0 defined in $K^-+p\rightarrow\Lambda+\pi^++\pi^-+M^0$. M^0 is obtained using the Λ momentum calculated with the constraint that it point to the K^-p vertex, together with the unfitted momenta of the positive and negative particles assumed to be pions. (a) $\sim$2150 Λ fits at 4.1 GeV/c. (b) $\sim$8500 Λ fits at 5.5 GeV/c. (c) and (d) Detailed view of the region around $M^0=0$ at 4.1 and 5.5 GeV/c, respectively.

hypotheses, or if they fit the $\Sigma^0\pi^+\pi^-$ or $\Sigma^0K^+K^-$ hypotheses with $M^2\leq 0$, or if they were among the $\Lambda\phi\pi^0$ events discussed in Sec. VIII. The only major ambiguity left to consider is the $\Lambda\pi^+\pi^-\eta$ hypothesis.

From an examination of the missing neutral mass distributions shown in Fig. 12, it is evident that the missing η hypothesis is a valid one. The number of real $\Lambda\pi^+\pi^-\eta$ events where the η decays into all neutral particles can also be estimated from those $\Lambda\pi^+\pi^-\eta$ events where the η decays into $\pi^+\pi^-\pi^0$ or $\pi^+\pi^-\gamma$.[14] In this manner we estimate the number of $\Lambda\pi^+\pi^-\eta$ events where the η decays into all neutral particles to be 60 ± 30 at 4.1 GeV/c and 330 ± 100 at 5.5 GeV/c, with less than half of these expected to give fits to the $\Lambda\pi^+\pi^-\pi^0$ hypothesis. This is consistent with the observed η peaks shown in Fig. 12.

The contamination from multineutrals was estimated from the asymmetry of the missing-mass-squared distribution about the value expected for a single missing π^0. The multineutral contamination gives an excess of events with a mass greater than one π^0 mass. The final number of $\Lambda\pi^+\pi^-\pi^0$ events estimated is 700 ± 100 at 4.1 GeV/c and 2000 ± 300 at 5.5 GeV/c.

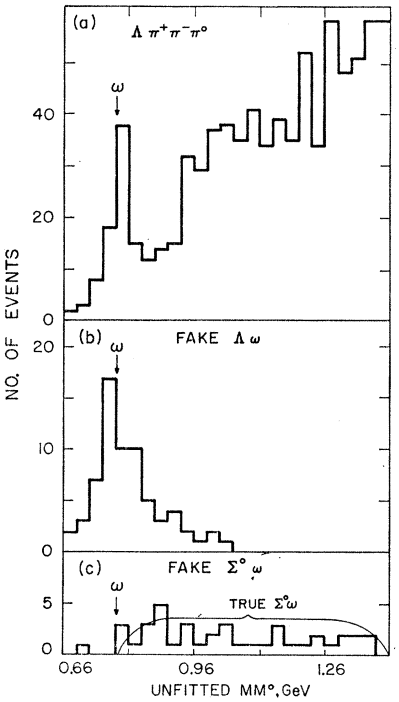

FIG. 13. The unfitted missing mass MM^0, defined in $K^-+p\rightarrow\Lambda+MM^0$ for (a) $\Lambda\pi^+\pi^-\pi^0$ fits, (b) $\Lambda\omega$ events generated by FAKE, and (c) $\Sigma^0\omega$ events generated by FAKE, all at 5.5 GeV/c. Without measurement errors true $\Sigma^0\omega$ events have MM^0 ranging from 0.79 to 1.35 GeV.

[14] D. Reeder, University of Wisconsin (private communication). We thank Professor Reeder and his co-workers for allowing us to use their results which are based on analysis of four-prong $+V$ events in the same film.

The ambiguities contained in the $\Lambda\omega$ events were considered in detail in Ref. 6. In particular, it was concluded that any $\Sigma^0\omega$ events contaminating the $\Lambda\omega$ peak were small in number and the same conclusion remains true for the present data. The essential point is that for $\Sigma^0\omega$ events the unfitted mass recoiling from the Λ does not give a sharp peak in the region of the ω, as can be seen in Fig. 13.

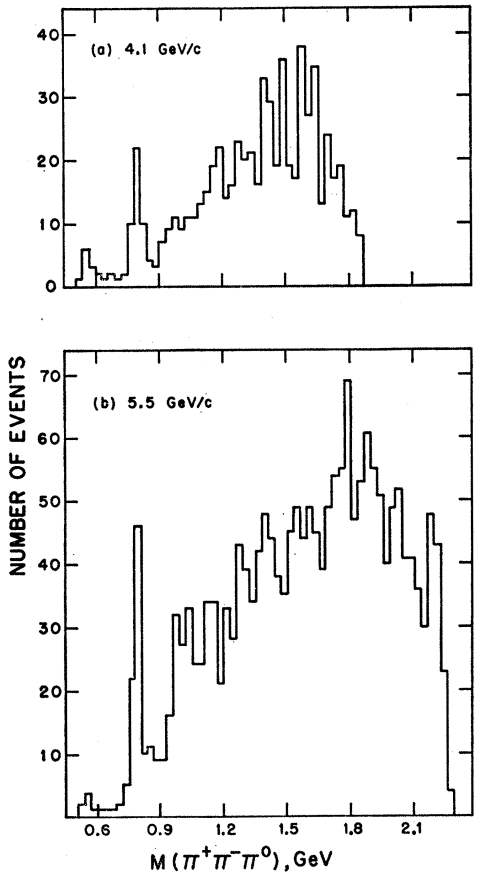

FIG. 14. The $\pi^+\pi^-\pi^0$ mass for a selection of $\Lambda\pi^+\pi^-\pi^0$ events after removal of: events fitting four-constraint hypotheses; events fitting the $\Sigma^0\pi^+\pi^-$ hypothesis with $M^2<0$, where M^2 is defined in $K^-+p\rightarrow\Lambda+\pi^++\pi^-+M$; all fits with $M>0.42$ GeV; and any $\Lambda\pi^+\pi^-\pi^0/\Lambda K^+K^-\pi^0$ ambiguities containing the $\Lambda\phi\pi^0$ events which had $\Delta^2(\phi)<1$ (GeV/c)^2 (see Fig. 27). (a) $\sim$700 events at 4.1 GeV/c. (b) $\sim$1900 events at 5.5 GeV/c.

B. Display of Data

The $\Lambda\omega$ final state can be seen in the mass histogram of Fig. 14 and the Chew-Low plots of Fig. 15. There is also a somewhat smaller signal for $\Lambda\eta$ in these plots. Evidence for ρ and $Y_1^*(1385)$ production can be seen in Figs. 16 and 17. Associated production of $Y^*\rho$ was then searched for. The $Y^{*+}\rho^-$ final state can be seen easily in the triangle plot in Fig. 18. The definition of associated production that we are using is an observation of an excess of events in the overlap region of the Y^* and ρ bands which is above that expected from the

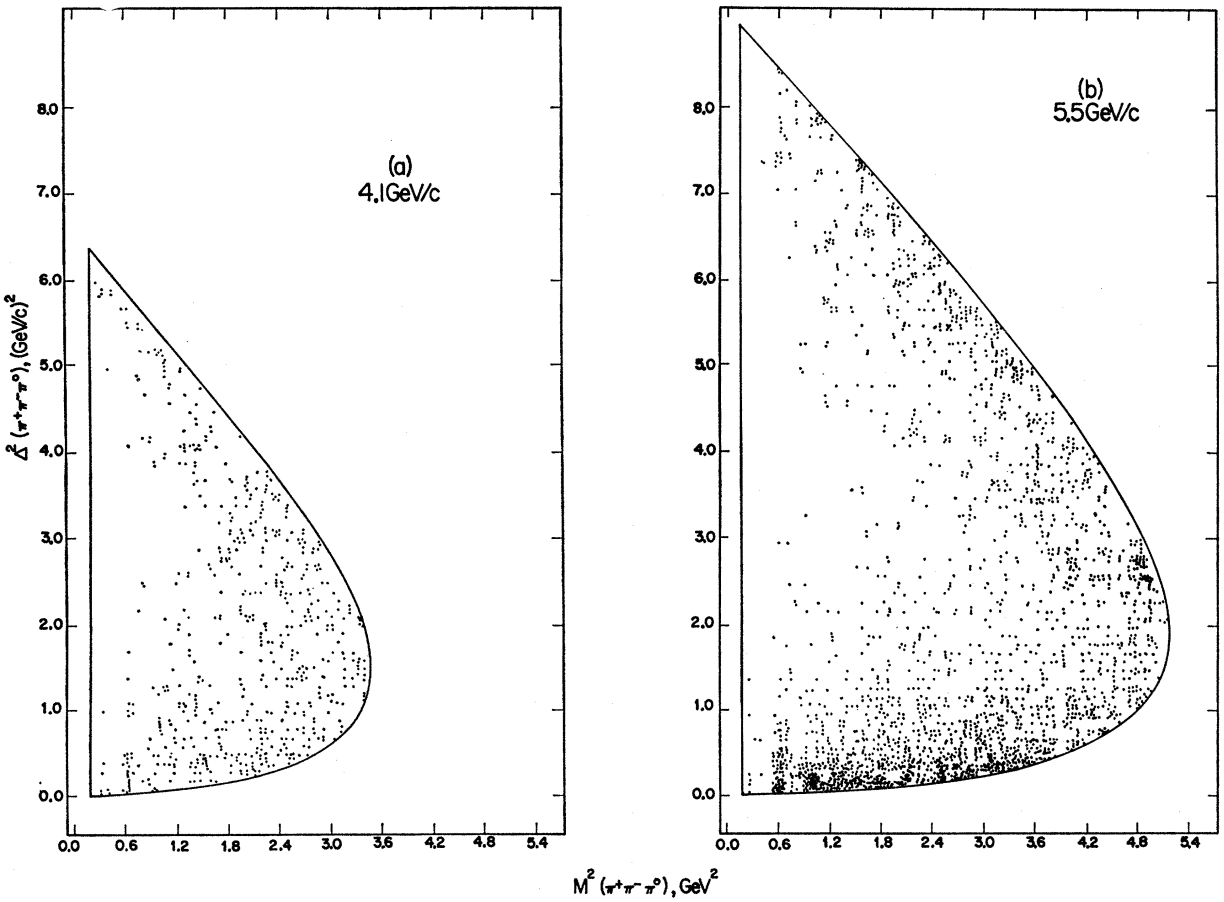

FIG. 15. Chew-Low plots for the $\pi^+\pi^-\pi^0$ system for the events described in Fig. 14. The events have been weighted as described in Sec. II B.

sum of the $Y^{*+}\pi^-\pi^0$ and $\Lambda\pi^+\rho^-$ events.[15] A small amount of $Y^{*0}\rho^0$ was found in a similar triangle plot in Fig. 19. The observation of ~ 70 $Y^{*+}\rho^-$ events at 5.5 GeV/c indicates that there should be ~ 17 $Y^{*0}\rho^0$ events assuming exchange of a half-unit of isospin. The 30 ± 20 $Y^{*0}\rho^0$ events which are observed satisfy this requirement within the limited statistics.

The production of $Y^{*-}\rho^+$ was investigated by selecting the $\Lambda\pi^-$ to be in the region of 1385 MeV and then looking at the production angular distribution of the meson system. In Fig. 20 an excess of ρ^+ events can be seen in the backward direction, presumably arising from baryon exchange. A comparison of similar distributions made when the $\Lambda\pi^-$ is not in the region of 1385 MeV indicates that the ρ^+ seen in Fig. 20 is essentially all associated with $Y_1^{*-}(1385)$. On the other hand, there is apparently no backward production of $Y_1^{*+}(1385)\rho^-$, as seen in a similar plot in Fig. 21.

Higher resonances decaying into the observed Y^* or ρ were searched for by making Dalitz plots of the quasi-three-body states $Y_1^{*+}(1385)\pi^-\pi^0$, $Y_1^{*0}(1385)\pi^+\pi^-$, $\Lambda\pi^+\rho^-$, $\Lambda\pi^0\rho^0$, and $\Lambda\pi^-\rho^+$. The final state involving Y^{*-} yielded no further information beyond the associated production of $Y^{*-}\rho^+$ previously discussed. At 5.5 GeV/c, it appears from the Dalitz plots of Figs. 22(a) and 22(b) that there is an enhancement at a mass ~ 1700 MeV in both the $Y_1^{*+}(1385)\pi^0$ and $Y_1^{*0}(1385)\pi^+$ final states. However, the situation is complicated by the fact that the $Y_1^{*+}(1385)$ and $Y_1^{*0}(1385)$ mass bands intersect in the middle of the $\Lambda\pi^+\pi^0$ Dalitz plot when the $\Lambda\pi^+\pi^0$ system has a mass of 1695 MeV, as shown in Fig. 22(c). In this case, there is the possibility of interference in the overlap region of $Y_1^{*+}(1385)$ and $Y_1^{*0}(1385)$. Furthermore, there is some evidence that the $Y_1^*(1660)$ decays through the $Y_1^*(1385)\pi$ mode.[16] Thus any attempt to interpret the enhancement in the $Y_1^*(1385)\pi$ mass spectrum at ~ 1700 MeV as being due to a $Y^*\pi$ decay mode of the $Y^*(1695)$ may be subject to large systematic errors. In any case the possible amount of $Y_1^{*0,+}(1385)\pi^{+,0}$ enhancement is

[15] This neglects any interference between the $Y^*\pi\pi$, $\Lambda\rho\pi$, $Y^*\rho$, and background amplitudes.

[16] W. H. Sims, Florida State University (private communication). Dr. Sims and co-workers at Florida State, Tufts, and Brandeis Universities have evidence for $Y_1^*(1660) \to Y_1^*(1385)\pi$ in a formation experiment which substantiates the $\frac{3}{2}^-$ assignment of the $Y_1^*(1660)$.

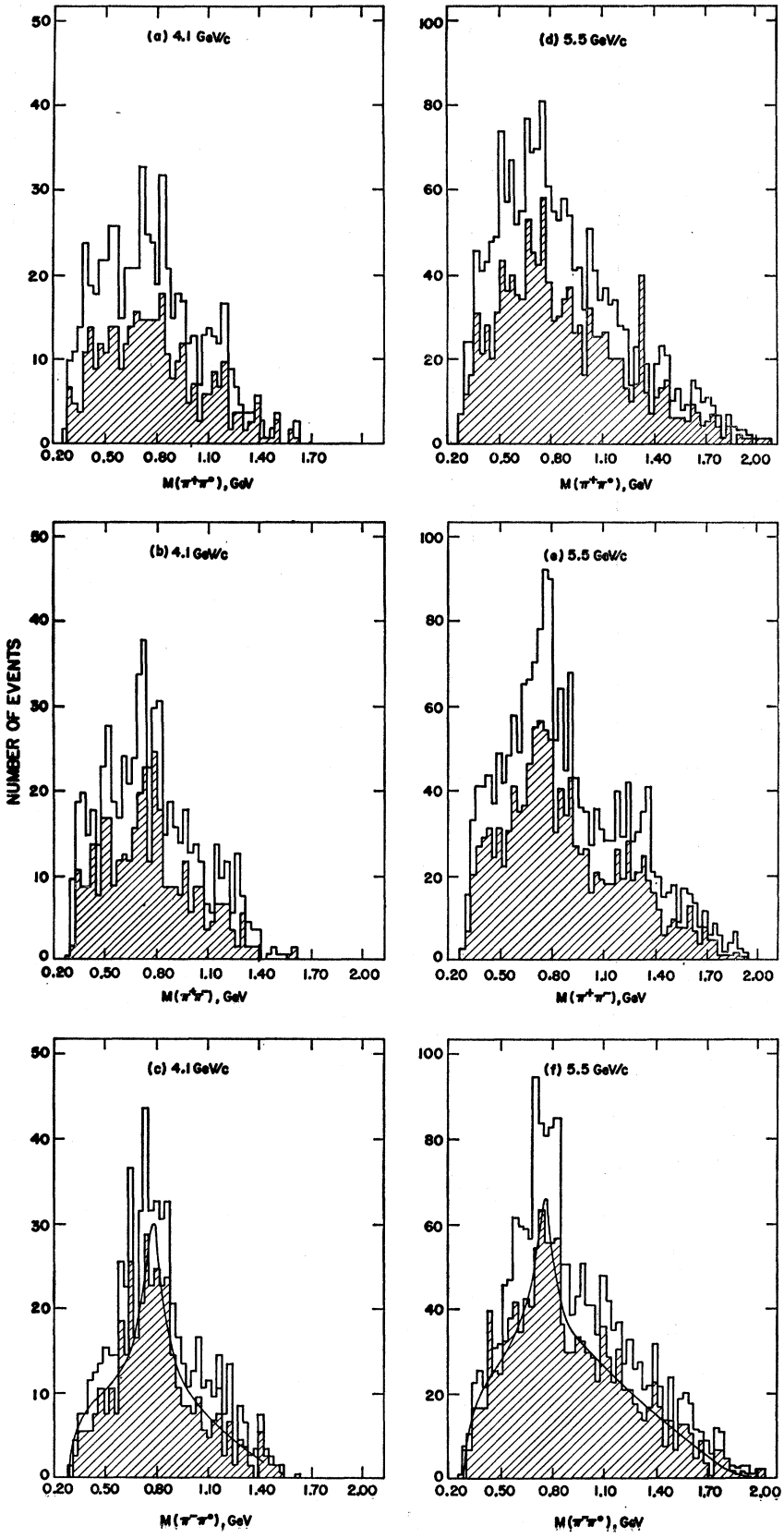

FIG. 16. Meson mass projections for the $\Lambda\pi^+\pi^-\pi^0$ final state. The events are the ones described in Fig. 14 and in addition have had $\Lambda\eta$ and $\Lambda\omega$ events removed. (a) The $\pi^+\pi^0$ mass at 4.1 GeV/c. The shaded area contains 353 events after subtraction of 314 $\Lambda\rho^0\pi^0$, $\Lambda\rho^-\pi^+$, $Y_1^{*+}(1385)\pi^-\pi^0$, $Y_1^{*0}(1385)\pi^+\pi^-$, and $Y_1^{*-}(1385)\pi^+\pi^0$ events. (b) The $\pi^+\pi^-$ mass at 4.1 GeV/c. The shaded area contains 369 events after subtraction of 298 $\Lambda\rho^+\pi^-$, $\Lambda\rho^-\pi^+$, $Y_1^{*+}(1385)\pi^-\pi^0$, $Y_1^{*0}(1385)\pi^+\pi^-$, and $Y_1^{*-}(1385)\pi^+\pi^0$ events. (c) The $\pi^-\pi^0$ mass at 4.1 GeV/c. The shaded area contains 418 events after subtraction of 249 $\Lambda\rho^+\pi^-$, $\Lambda\rho^0\pi^0$, $Y_1^{*+}(1385)\pi^-\pi^0$, $Y_1^{*0}(1385)\pi^+\pi^-$, and $Y_1^{*-}(1385)\pi^+\pi^0$ events. The solid curve is a best fit to the shaded histogram for phase space and one Breit-Wigner resonance for the ρ^- using the mass and width given in Ref. 13. The relative contributions are 72% phase space and 28% ρ^-. (d) The $\pi^+\pi^0$ mass at 5.5 GeV/c. The shaded area contains 1148 events after subtraction of 717 $\Lambda\rho^0\pi^0$, $\Lambda\rho^-\pi^+$, $Y_1^{*+}(1385)\pi^-\pi^0$, $Y_1^{*0}(1385)\pi^+\pi^-$, and $Y_1^{*-}(1385)\pi^+\pi^0$ events. (e) The $\pi^+\pi^-$ mass at 5.5 GeV/c. The shaded area contains 1190 events after subtraction of 675 $\Lambda\rho^+\pi^-$, $\Lambda\rho^-\pi^+$, $Y_1^{*+}(1385)\pi^-\pi^0$, $Y_1^{*0}(1385)\pi^+\pi^-$, and $Y_1^{*-}(1385)\pi^+\pi^0$ events. (f) The $\pi^-\pi^0$ mass at 5.5 GeV/c. The shaded area contains 1296 events after subtraction of 569 $\Lambda\rho^+\pi^-$, $\Lambda\rho^0\pi^0$, $Y_1^{*+}(1385)\pi^-\pi^0$, $Y_1^{*0}(1385)\pi^+\pi^-$, and $Y_1^{*-}(1385)\pi^+\pi^0$ events. The solid curve is a best fit to the shaded histogram for phase space and one Breit-Wigner resonance for the ρ^- using the mass and width given in Ref. 13. The relative contributions are 84% phase space and 16% ρ^-.

TABLE V. Cross sections derived from $\Lambda\pi^+\pi^-\pi^0$ events.

Reaction channel	Total No. of events 4.1 GeV/c	Total No. of events 5.5 GeV/c	Weighted No. of events[a] 4.1 GeV/c	Weighted No. of events[a] 5.5 GeV/c	σ (μb) for decay into particles observed 4.1 GeV/c	σ (μb) for decay into particles observed 5.5 GeV/c	σ (μb) corrected for other decay modes[b] 4.1 GeV/c	σ (μb) corrected for other decay modes[b] 5.5 GeV/c
$\Lambda\pi^+\pi^-\pi^0$	700±100	2000±300	640±105	2260±389	1050±214	465±85		
$\Lambda\eta$ → $\pi^+\pi^-\pi^0$	8± 4	3± 3	8± 5	3± 3	13± 8	0.6±0.6	48±30	2± 2
$\Lambda\omega$ → $\pi^+\pi^-\pi^0$	37± 8	80± 10	30± 7	92± 13	49± 13	19± 3	54±14	21± 3
ΛA_2^0 → $\rho^-\pi^+$	<5	<10	<5	<10	<8	<2	<18	<5
$Y_1^{*+}(1385)\rho^-$ → $\Lambda\pi^+$	35± 17	70± 25	39± 22	74± 30	64± 37	15± 6	70±41	16± 7
$Y_1^{*0}(1385)\rho^0$ → $\Lambda\pi^0$	13± 15	30± 20	13± 17	30± 23	21± 27	6± 5	23±30	7± 6
$Y_1^{*-}(1385)\rho^+$ → $\Lambda\pi^-$			15± 8	30± 14	25± 14	6± 3	27±15	7± 3
$Y_1^{*+}(1385)\pi^-\pi^0$ → $\Lambda\pi^+$	88± 33	280± 52	72± 31	296± 63	118± 53	61±14	130±58	67±15
$Y_1^{*0}(1385)\pi^+\pi^-$ → $\Lambda\pi^0$	75± 33	149± 54	75± 38	149± 62	123± 64	31±13	135±70	34±14
$Y_1^{*-}(1385)\pi^+\pi^0$ → $\Lambda\pi^-$	31± 35	37± 58	25± 32	43± 78	41± 53	9±16	45±58	10±18
$\Lambda\rho^+\pi^-$	50± 41	186± 63	46± 43	212± 83	75± 71	44±33	75±71	44±33
$\Lambda\rho^0\pi^0$	69± 46	243± 75	64± 49	271± 96	106± 82	56±20	106±82	56±20
$\Lambda\rho^-\pi^+$	176± 36	299± 60	163± 38	352± 81	267± 70	73±17	267±70	73±17

[a] Calculated as described in Sec. II B, using events from a restricted fiducial volume containing ~20% less events than the observed total of the previous column.
[b] Reference 13.
[c] Numbers quoted for ΛA_2 are at the 70% confidence level.

TABLE VI. The ΛX^0 cross sections.

Observed particles	Total No. of events 4.1 GeV/c	Total No. of events 5.5 GeV/c	Weighted No. of events[a] 4.1 GeV/c	Weighted No. of events[a] 5.5 GeV/c	σ (μb) for decay into particles observed 4.1 GeV/c	σ (μb) for decay into particles observed 5.5 GeV/c	σ (μb) corrected for other decay modes[b] 4.1 GeV/c	σ (μb) corrected for other decay modes[b] 5.5 GeV/c
$\Lambda\pi^+\pi^-\eta$ → all neutral	15±4	31±6	14±4	31±6	23±6	7±2	72±20	20±4
$\Lambda\rho^0\gamma$		20±6		20±6		4±2		

[a] Calculated as described in Sec. II B, using events from a restricted fiducial volume containing ~20% less events than the observed total of the previous column.
[b] Reference 13.

TABLE VII. Cross sections derived from the $\Lambda K^+K^-\pi^0$ events.

Reaction channel	Total No. of events 4.1 GeV/c	Total No. of events 5.5 GeV/c	Weighted No. of events[a] 4.1 GeV/c	Weighted No. of events[a] 5.5 GeV/c	σ (μb) for decay into particles observed 4.1 GeV/c	σ (μb) for decay into particles observed 5.5 GeV/c	σ (μb) corrected for other decay modes[b] 4.1 GeV/c	σ (μb) corrected for other decay modes[b] 5.5 GeV/c
$\Lambda\phi\pi^0$	18±6	78±15	18±7	80±17	30±12	17±3	64±26	36±6
$Y_1^{*0}(1385)\phi$	3±3	18± 5	3±3	18± 6	5± 5	4±2	12±12	9± 5

[a] Calculated as described in Sec. II B, using events from a restricted fiducial volume containing ~20% less events than the observed total of the previous column.
[b] Reference 13.

best estimated from Fig. 23, where events in the overlap region of $Y_1^{*+}(1385)$ and $Y_1^{*0}(1385)$ have only been counted once and $\Lambda\pi\rho$ have been removed.

We now turn our attention to the $\Lambda\pi\rho$ final states. Dalitz plots of the $\Lambda\pi^+\rho^-$ are shown in Fig. 24. We note that there is an absence of strong A_2 production in the $\pi^+\rho^-$ projection. Dalitz plots of $\Lambda\pi^{0,-}\rho^{0,+}$ events have also been examined but are complicated by the fact that the strong $\Lambda\pi^+\rho^-$ production simulates an enhancement in the $\pi^{-,0}\rho^{+,0}$ system at the A_2 mass.[13]

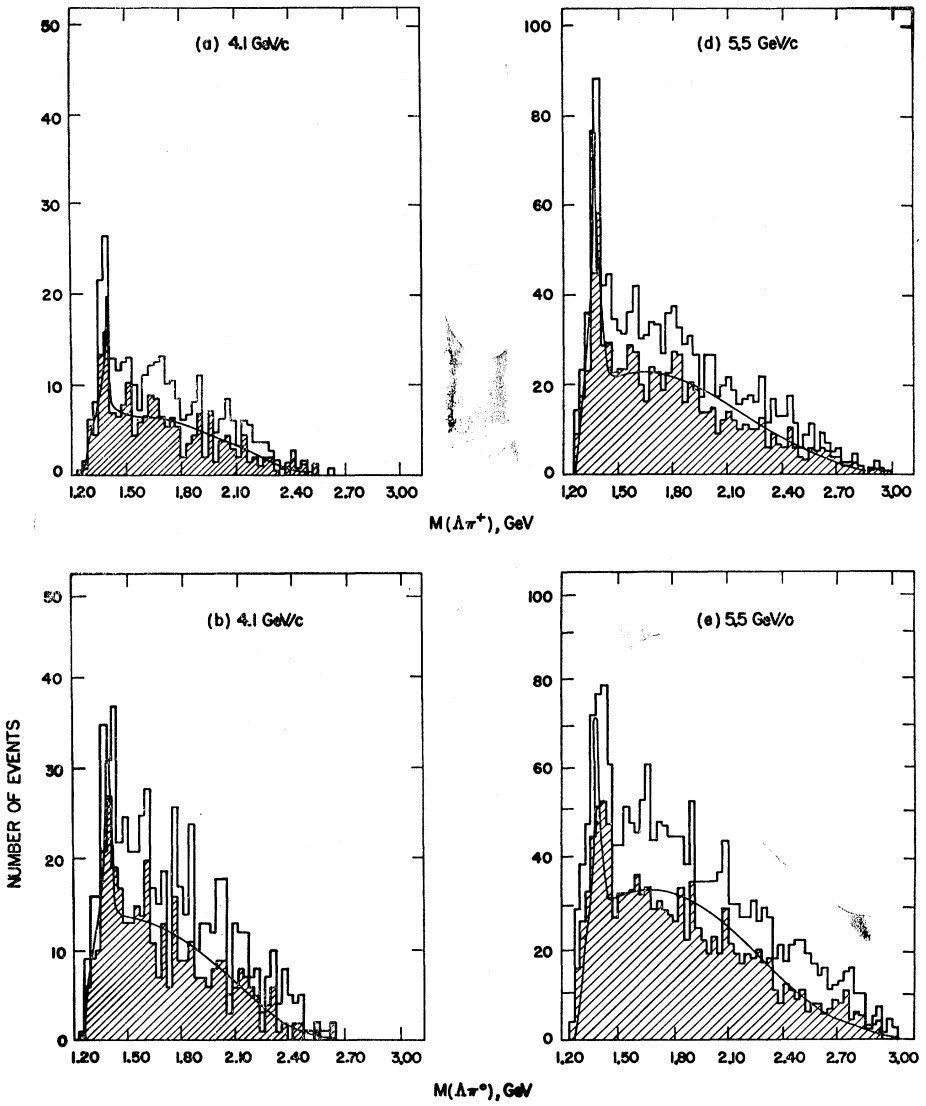

FIG. 17. Bayron mass projections for the $\Lambda\pi^+\pi^-\pi^0$ final state. The events are the ones described in Fig. 14 and in addition have had $\Lambda\eta$ and $\Lambda\omega$ events removed. (a) The $\Lambda\pi^+$ mass at 4.1 GeV/c. The shaded area contains 377 events after subtraction of 290 $\Lambda\rho^+\pi^-$, $\Lambda\rho^0\pi^0$, $\Lambda\rho^-\pi^+$, $Y_1^{*0}(1385)\pi^+\pi^-$, and $Y_1^{*-}(1385)\pi^+\pi^0$ events. The solid curve is a best fit to the shaded histogram for phase space and one Breit-Wigner resonance for the $Y_1^{*+}(1385)$ using the mass and width given in Ref. 13. The relative contributions are 86% phase space and 14% $Y_1^{*+}(1385)$. (b) The $\Lambda\pi^0$ mass at 4.1 GeV/c. The shaded area contains 369 events after subtraction of 298 $\Lambda\rho^+\pi^-$, $\Lambda\rho^0\pi^0$, $\Lambda\rho^-\pi^+$, $Y_1^{*+}(1385)\pi^-\pi^0$, and $Y_1^{*-}(1385)\pi^+\pi^0$ events. The solid curve is a best fit to the shaded histogram for phase space and one Breit-Wigner resonance for the $Y_1^{*0}(1385)$ using the mass and width given in Ref. 13. The relative contributions are 88% phase space and 12% $Y_1^{*0}(1385)$. (c) The $\Lambda\pi^-$ mass at 4.1 GeV/c. The shaded area contains 345 events after subtraction of 322 $\Lambda\rho^+\pi^-$, $\Lambda\rho^0\pi^0$, $\Lambda\rho^-\pi^+$, $Y_1^{*+}(1385)\pi^-\pi^0$, and $Y_1^{*0}(1385)\pi^+\pi^-$ events. The solid curve is a best fit to the shaded histogram for phase space and one Breit-Wigner resonance for the $Y_1^{*-}(1385)$ using the mass and width given in Ref. 13. The relative contributions are 95% phase space and 5% $Y_1^{*-}(1385)$. (d) The $\Lambda\pi^+$ mass at 5.5 GeV/c. The shaded area contains 1212 events after subtraction of 653 $\Lambda\rho^+\pi^-$, $\Lambda\rho^0\pi^0$, $\Lambda\rho^-\pi^+$, $Y_1^{*0}(1385)\pi^+\pi^-$, and $Y_1^{*-}(1385)\pi^+\pi^0$ events. The solid curve is a best fit to the shaded histogram for phase space and one Breit-Wigner resonance for the $Y_1^{*+}(1385)$ using the mass and width given in Ref. 13. The relative contributions are 85% phase space and 15% $Y_1^{*+}(1385)$. (e) The $\Lambda\pi^0$ mass at 5.5 GeV/c. The shaded area contains 1176 events after subtraction of 689 $\Lambda\rho^+\pi^-$, $\Lambda\rho^0\pi^0$, $\Lambda\rho^-\pi^+$, $Y_1^{*+}(1385)\pi^-\pi^0$, and $Y_1^{*-}(1385)\pi^+\pi^0$ events. The solid curve is a best fit to the shaded histogram for phase space and one Breit-Wigner resonance for the $Y_1^{*0}(1385)$ using the mass and width given in Ref. 13. The relative contributions area 92% phase space and 8% $Y_1^{*0}(1385)$. (f) The $\Lambda\pi^-$ mass at 5.5 GeV/c. The shaded area contains 1118 events after subtraction of 747 $\Lambda\rho^+\pi^-$, $\Lambda\rho^0\pi^0$, $\Lambda\rho^-\pi^+$, $Y_1^{*+}(1385)\pi^-\pi^0$, and $Y_1^{*0}(1385)\pi^+\pi^-$ events. The solid curve is a best fit to the shaded histogram for phase space and one Breit-Wigner for the $Y_1^{*-}(1385)$ using the mass and width given in Ref. 13. The relative contributions are 90% phase space and 10% $Y_1^{*-}(1385)$.

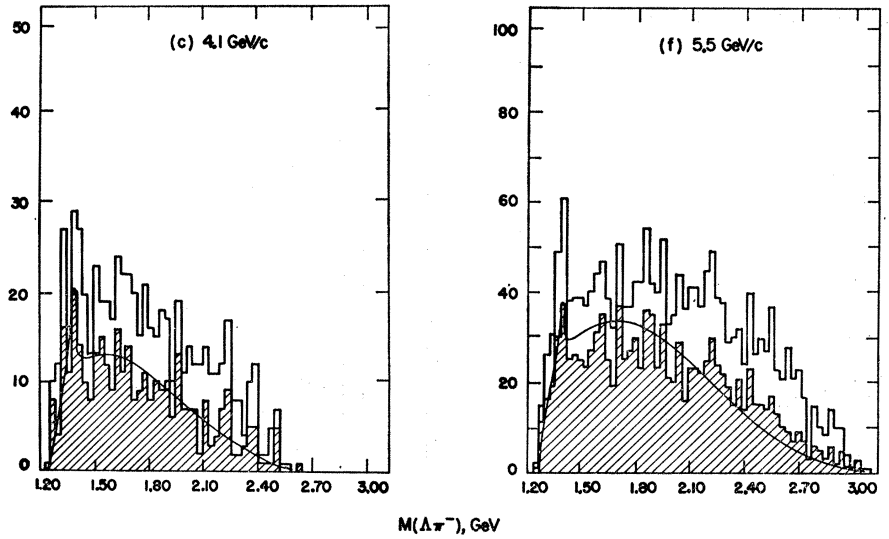

FIG. 17. (*continued*).

TABLE VIII. Cross sections for production in the backward hemisphere.

Final states	σ_B (μb) corrected for decay modes not observed in this expt.[a] 4.1 GeV/c	5.5 GeV/c
$\Lambda\rho^0$	32±17	7±3
$\Lambda\phi$	<6[a]	<1[b]
$\Lambda f^* \searrow K\bar{K}$	<6[a,b]	<1[b,c]
$\Lambda\omega$	3±3	4±2
ΛX^0	<10[a]	<2[a]
$Y_1^{*+}(1385)\pi^-$	<3[a]	2±1
$Y_1^{*+}(1385)\rho^-$	18±9	<2[a]
$Y_1^{*-}(1385)\pi^+$	8±8	1±1
$Y_1^{*-}(1385)\rho^+$	27±15	7±3
$Y_1^{*+}(1695)\pi^- \searrow \Lambda\pi^+$	<3[a,b]	3±3[b]

[a] Reference 13.
[b] All upper limits are at the 70% confidence level.
[c] Estimated only for the decay modes indicated.

Cross sections for all of the above states are summarized in Table V.

VII. KINEMATIC FITS TO THE $\Lambda\pi^+\pi^-\eta$ AND $\Lambda\pi^+\pi^-\gamma$ HYPOTHESES: ΛX^0 FINAL STATE

Figure 12 shows distributions of the unfitted neutral missing mass M^0 in the reaction $K^-+p\to\Lambda+\pi^+ +\pi^-+M^0$ for all events with an identified Λ. From this it is evident that there are a significant number of events with a missing η. Thus our sample of $\Lambda\pi^+\pi^-\eta$ fits will include events with a genuine missing η in addition to spurious fits carved out of the multineutral continuum by the kinematic fitting program.

The kinematic fits to the $\Lambda\pi^+\pi^-\eta$ hypothesis were unique when the $\pi^+\pi^-\eta$ invariant mass was near the X^0 mass. In Fig. 25 the distribution of the $\pi^+\pi^-\eta$ invariant mass, when the missing mass lies between 0.5 and 0.6 GeV, is presented along with background estimates made from events in neighboring regions. The X^0 events were entirely peripheral with no backward peak as seen in the Chew-Low plots of Fig. 26.

In addition to the hypotheses listed in Table I, we also tried the hypothesis $\Lambda\pi^+\pi^-\gamma$ on all events for which the mass recoiling against the Λ lies between 0.66 and 1.26 GeV. In this manner it was possible to study the

TABLE IX. Density matrix elements in the Λ+vector-meson final states.

Final state	Incident momentum (GeV/c)	ρ_{11}	ρ_{1-1}	Reρ_{10}
$\Lambda\rho^0$	4.1	0.40±0.06	−0.10±0.11	−0.12±0.07
	5.5	0.47±0.03	−0.19±0.08	−0.08±0.05
$\Lambda\omega$	4.1	0.50±0.07	0.25±0.17	−0.12±0.09
	5.5	0.30±0.06	0.11±0.10	−0.17±0.06
$\Lambda\phi$	4.1	0.16±0.13	0.25±0.16	−0.10±0.11
	5.5	0.35±0.07	0.17±0.12	0.02±0.08

TABLE X. Density matrix elements in the $Y_1^{*+}(1385)\pi^-$ final state.

	ρ_{33} 4.1 GeV/c	5.5 GeV/c	Reρ_{3-1} 4.1 GeV/c	5.5 GeV/c	Reρ_{31} 4.1 GeV/c	5.5 GeV/c
This experiment	0.28±0.09	0.22±0.06	0.15±0.09	0.14±0.06	0.19±0.10	0.06±0.05
Stodolsky-Sakurai prediction	0.375		0.216		0	
Absorption-model prediction	0.26	0.27	0.21	0.22	−0.09	−0.07

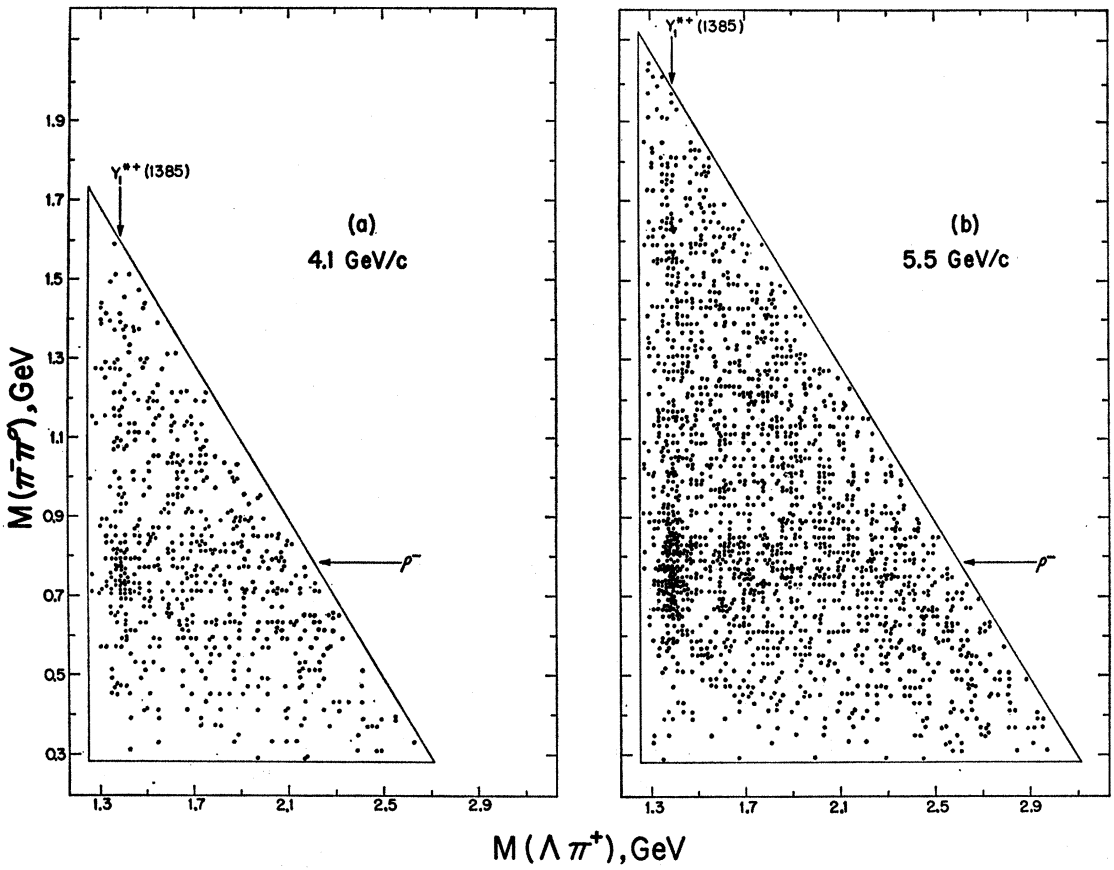

FIG. 18. Triangle plots showing the $Y^{*+}\rho^-$ enhancement. The events are those described in Fig. 14 and in addition have had $\Lambda\eta$ and $\Lambda\omega$ events removed.

decay $X^0 \to \pi^+\pi^-\gamma$. For such events the principal ambiguity is with the $\Lambda\pi^+\pi^-\pi^0$ hypothesis. A detailed discussion of our X^0 results, including a treatment of ambiguities, has already been presented elsewhere[17] and is summarized in Sec. IX E.

Cross sections for the ΛX^0 final state are given in Table VI.

VIII. KINEMATIC FITS TO THE $\Lambda K^+K^-\pi^0$ HYPOTHESIS: $Y_1^{*0}(1385)\phi$ FINAL STATE

The $\Lambda K^+K^-\pi^0$ fits at 5.5 GeV/c show strong evidence of peripheral ϕ production as may be seen in Fig. 27, where a Chew-Low plot for the K^+K^- system is presented along with a projection of the plot onto the mass axis. A very sharp ϕ peak is evident and may be readily isolated from the background by a forward peripheral cut, as indicated in the figure.

For these events, the ambiguities were primarily with the $\Lambda\pi^+\pi^-\pi^0$ and the $\Lambda\pi^+\pi^-\eta$ hypotheses. The interpretation is further complicated by the fact that when events which have a K^+K^- invariant mass lying between 1000 and 1040 MeV are interpreted as $\pi^+\pi^-$, one obtains a $\pi\pi$ invariant mass between about 325 and 430 MeV. Thus the peaking in the invariant-mass distribution of the two charged particles is subject to alternate interpretations either as $\phi \to K^+K^-$ or as a possible "σ enhancement" in the $\pi^+\pi^-$ system. The ambiguities were resolved by looking at the mass of the missing neutral which is expected to be the π^0 or η when the two charged particles are interpreted as $\pi^+\pi^-$ and is expected to be the π^0 when two charged particles are interpreted as K^+K^-. The mass distribution of the missing neutral showed no peak at all in the former case, but showed a sharp π^0 peak in the latter case, indicating that the events as a whole were $\Lambda\phi\pi^0$ and they were so assigned.

The reaction $K^- + p \to Y_1^{*0}(1385) + \phi$ clearly occurs at 5.5 GeV/c, as can be seen in the Dalitz plot of Fig. 28.

The cross sections for $\Lambda\phi\pi^0$ and $Y_1^{*0}(1385)\phi$ at both momenta are given in Table VII.

IX. DISCUSSION AND CONCLUSIONS

A. General Characteristics of Two-Body Final States

A general feature of these data is that for two-body final states the production angular distribution of the meson system is forward peaked as expected from a

[17] R. E. P. Davis, R. Ammar, J. Mott, S. Dagan, M. Derrick, and T. Fields, Phys. Letters **27B**, 532 (1968).

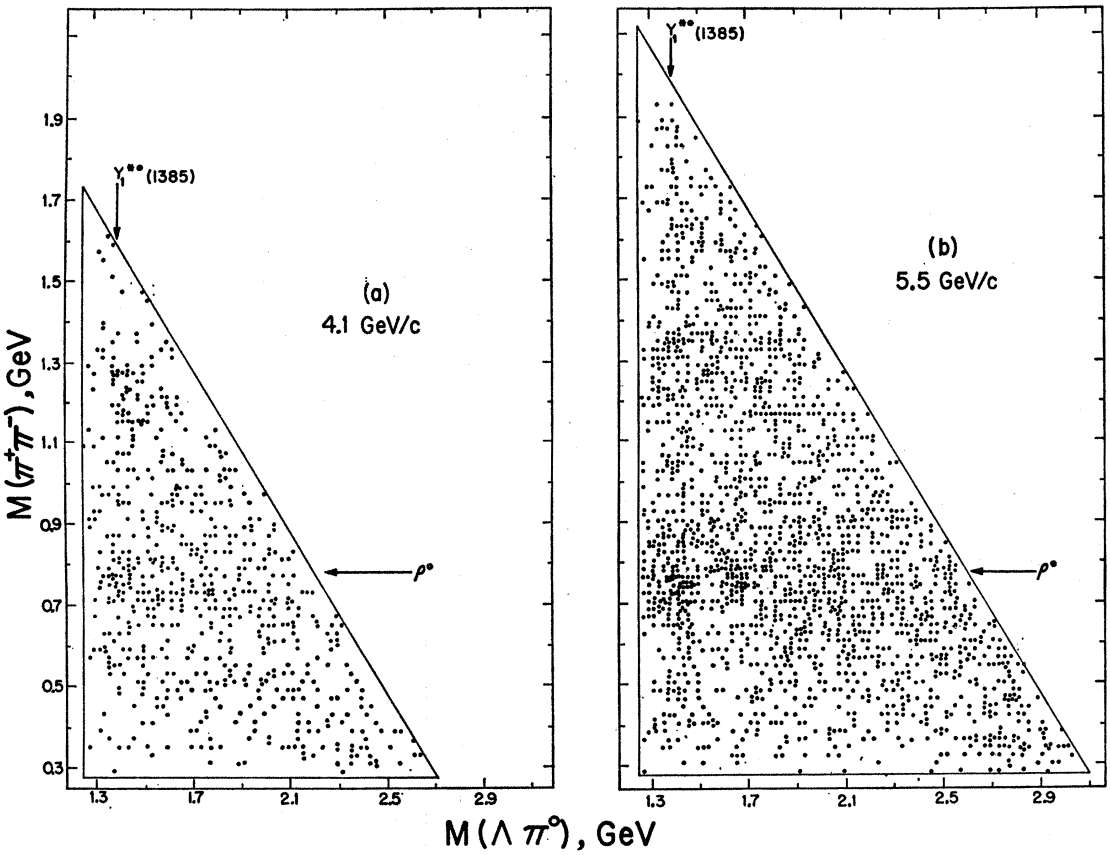

FIG. 19. Triangle plots showing the $Y^{*0}\rho^0$ enhancement. The events are the same as those in Fig. 14 and in addition have had $\Lambda\eta$ and $\Lambda\omega$ events removed.

single-meson-exchange process. This is seen in Fig. 29 for the Λ+meson final states. In some cases there is also a small backward peak, indicating that baryon exchange occurs as a less frequent production process.

In the case of the $\Lambda\phi$ and ΛX^0 final states, the backward peak seems to be completely absent. The lack of a backward peak in the $\Lambda\phi$ final state has also been observed in 3.0 GeV/c (Ref. 2) and 3.5 GeV/c (Ref. 3) K^-p interactions and indicates a weak $N\bar{N}\phi$ coupling in agreement with quark and ω-ϕ mixing models.[18] Combining the data at 4.1 and 5.5 GeV/c, the following 90% confidence limit for production in the backward hemisphere is obtained:

$$\sigma_B(K^-p\rightarrow\Lambda\phi)\leq 0.15\sigma_B(K^-p\rightarrow\Lambda\omega).$$

The production of $Y^{*+}\pi^-$ and $Y^{*+}\rho^-$ final states show characteristics similar to the Λ+meson reactions, as can be seen in Fig. 30.

The $Y_1^{*+}(1385)$ resonance decaying into $\Lambda\pi^+$ is copiously produced at both 4.1 and 5.5 GeV/c, as shown in Figs. 3 and 4. The dominance of one-meson exchange over baryon exchange is also consistent with the fact that the negative member of the isospin multiplet, $Y_1^{*-}(1385)$, which cannot be produced via the exchange of any single known meson, is not seen at either momenta although it can be produced by baryon exchange.

The only Y^* final state in which baryon exchange appears to be important is $Y_1^{*-}(1385)\rho^+$ production. This is also seen in the 6-GeV/c data.[4] In comparison $Y^{*-}\pi^+$ production is relatively small. These processes can proceed by either N or Δ exchange, but Δ exchange does not appear to be important since backward $Y^{*+}\pi^-$ and $Y^{*+}\rho^-$ production, which can only proceed via Δ exchange, have zero cross sections within errors. One therefore concludes that the $N\bar{N}\rho$ coupling is larger than $N\bar{N}\pi$ at a momentum transfer of ~ 7 (GeV/c)^2.

A summary of the backward cross sections is given in Table VIII.

In addition to the peripheral nature of the angular distributions, one observes a marked falloff of the two-body cross sections with increasing beam momentum as previously observed.[19]

[18] H. M. Fried and J. G. Taylor, Phys. Rev. Letters **15**, 709 (1965); N. J. Papastamatiou, Nuovo Cimento **41**, A625 (1966).

[19] M. Derrick, L. Hyman, J. Loken, T. Fields, F. Schweingruber, R. Ammar, R. E. P. Davis, J. Mott, and C. Sun, in *Proceedings of the Second Topical Conference on Resonant Particles, Athens, Ohio, 1965*, edited by B. A. Munir (Ohio University Press, Athens, Ohio, 1965), p. 325; D. R. O. Morrison, CERN Report No. CERN/TC/PHYSICS 66-20, 1966 (unpublished).

B. Exchange Mechanism in the $\Lambda\rho^0$, $\Lambda\omega$, and $\Lambda\phi$ Final States

Because of the forward peaking in the $\Lambda\rho^0$, $\Lambda\omega$, and $\Lambda\phi$ final states the production mechanism can be analyzed by means of a one-meson-exchange model. For the vector mesons considered, the angular distribution of the decay of the meson resonance is[20]

$$W_1(\theta,\phi)=C[\rho_{11}\sin^2\theta+(1-2\rho_{11})\cos^2\theta-\rho_{1-1}\sin^2\theta\cos2\phi-\sqrt{2}\,\mathrm{Re}\rho_{10}\sin2\theta\cos\phi].$$

For a two-body decay such as $\rho^0\to\pi^+\pi^-$, the angles θ and ϕ are the usual polar and azimuthal angles of the decay pion in the rest system of the resonance, the z axis being taken as the direction of the incident K^-, the y axis as the direction of the normal to the production plane, and the x axis completing the right-handed coordinate system. In the case of the ω which is observed in the three-pion decay mode, the angles θ and ϕ are the polar and azimuthal angles of the normal to the decay plane in the rest system of the resonance.

The average values of $\cos^2\theta$, $\sin^2\theta\cos2\phi$, and $\sin2\theta\times\cos\phi$ were found from the experimental data and the values of ρ_{11}, ρ_{1-1}, and $\mathrm{Re}\rho_{10}$ were obtained in the usual manner.[21] The results are summarized in Table IX. It is seen that ρ_{11} is usually near its maximum value of 0.5. In cases where the exchanged particles have natural parity and no absorption is present, $2\rho_{11}$ is the fraction of vector-particle-exchange process and $1-2\rho_{11}$ the fraction of pseudoscalar-particle-exchange process. However, in the present experimental data, absorption effects appear to be important since the dependence of the differential cross sections on momentum transfer are more sharply peaked than one would expect from the propagator of the exchanged particle. Figure 31 illustrates this fact for the data available at 5.5 GeV/c. In these cases the $\Lambda\rho$ and $\Lambda\omega$ data are consistent with $d\sigma/dt\sim\exp(-3|t|)$.

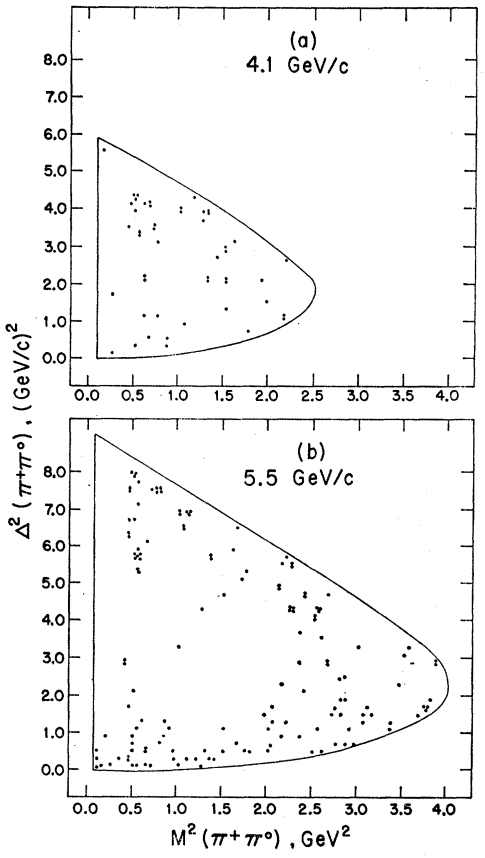

FIG. 20. Chew-Low plots for the $\pi^+\pi^0$ system for a selection of $\Lambda\pi^+\pi^-\pi^0$ events with the $\Lambda\pi^-$ mass in the region of 1385 MeV. The events have been weighted as described in Sec. II B.

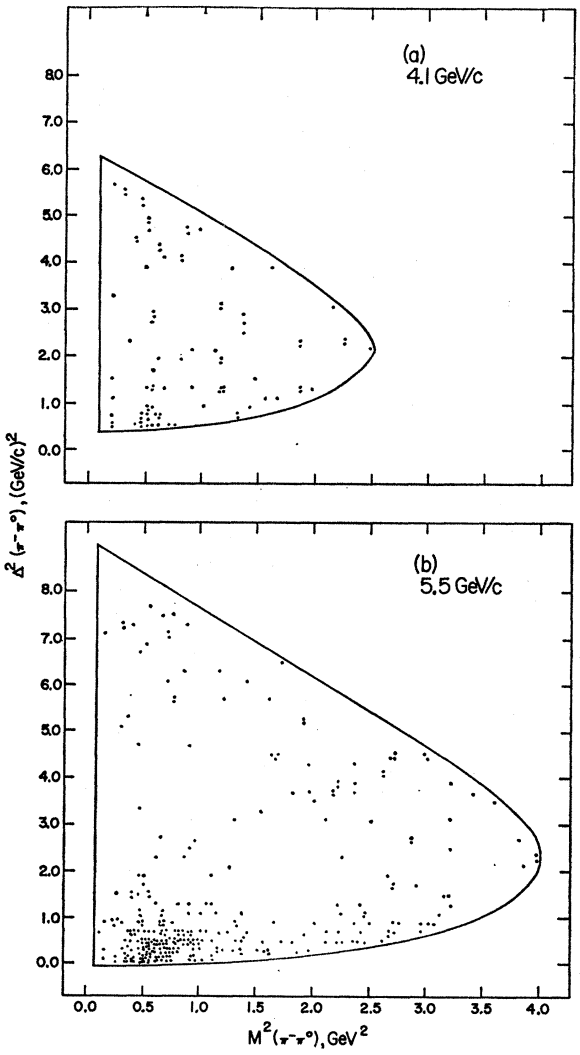

FIG. 21. Chew-Low plots for the $\pi^-\pi^0$ system for a selection of $\Lambda\pi^+\pi^-\pi^0$ events with the $\Lambda\pi^+$ mass in the region of 1385 MeV. The events have been weighted as described in Sec. II B.

[20] K. Gottfried and J. D. Jackson, Nuovo Cimento 33, 309 (1964).

[21] N. Schmitz, in Proceedings of the 1965 Easter School for Physicists, CERN Report No. CERN-65-24, 1965.

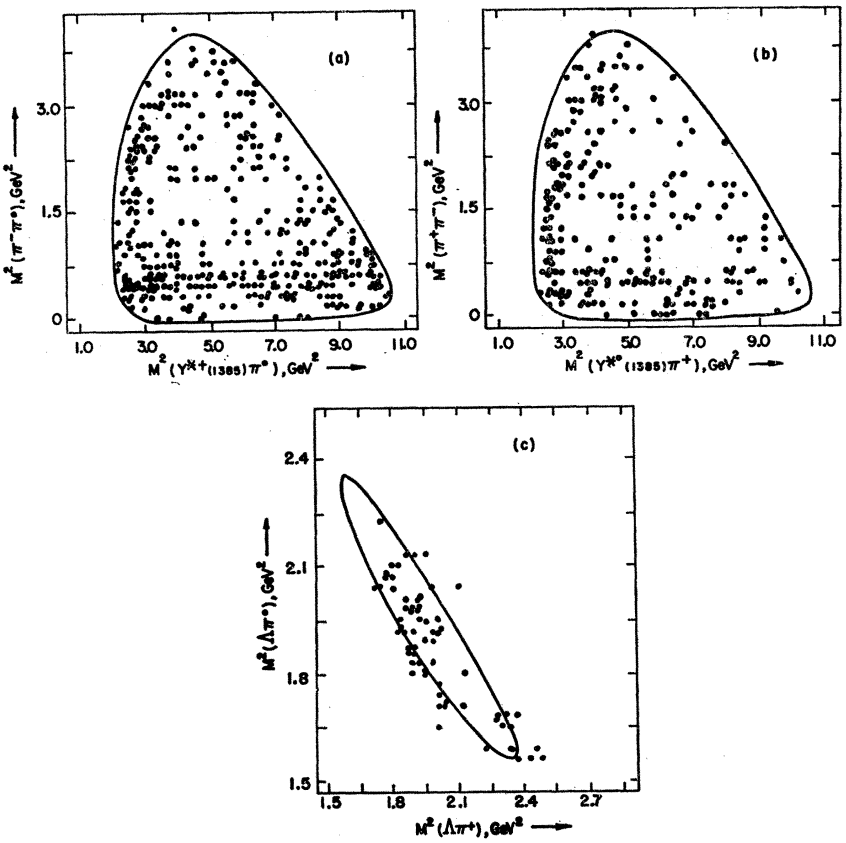

FIG. 22. (a) and (b) are Dalitz plots of the $Y_1^{*0,+}(1385)\pi^{+,0}\pi^-$ system contained in the $\Lambda\pi^+\pi^-\pi^0$ fits at 5.5 GeV/c. (c) Dalitz plot of the $\Lambda\pi^+\pi^0$ system for those $\Lambda\pi^+\pi^-\pi^0$ fits at 5.5 GeV/c for which the $\Lambda\pi^+\pi^0$ have the invariant mass of the $Y_1^{*+}(1695)$ and $\Delta^2<1$ (GeV/c)^2.

C. Systematics of $Y_1^{*+}(1385)\pi^-$, $Y_1^{*+}(1385)\rho^-$, and $Y_1^{*0}(1385)\phi$ Production

In general for a spin-$\frac{3}{2}$ resonance the decay angular distribution expected is[20]

$$W_{3/2}(\theta,\phi)=C[\rho_{33}\sin^2\theta+(\tfrac{1}{2}-\rho_{33})(\tfrac{1}{3}+\cos^2\theta) -\tfrac{2}{3}\sqrt{3}\,\mathrm{Re}\rho_{3-1}\sin^2\theta\cos2\phi-\tfrac{2}{3}\sqrt{3}\,\mathrm{Re}\rho_{31}\sin2\theta\cos\phi].$$

The coordinate system is similar to the one defined in Sec. IX B except that the z direction is now defined as the direction of the incident baryon in the c.m. system of the resonance.

Stodolsky and Sakurai[9] have treated baryon resonance production by analogy with the photoproduction of pions in the reaction $\gamma N\to N^*\to N\pi$ which is dominated by the $M1$ magnetic dipole transition. The assumption of vector-meson exchange in the production process with $M1$ dominance makes definite predictions for the density matrix elements for the decay of a $\frac{3}{2}^+$ resonance, namely,

$$\rho_{33}=\tfrac{3}{8}=0.375,\quad \mathrm{Re}\rho_{3-1}=\tfrac{1}{8}\sqrt{3}=0.216,\quad \mathrm{Re}\rho_{31}=0$$

with the corresponding decay angular distribution

$$W_{3/2^+}(\theta,\phi)=C'(1+3\sin^2\theta\sin^2\phi) =C'(1+3\cos^2\theta'),$$

where for simplicity the angular distribution has been parametrized in terms of θ' the angle of the decay pion

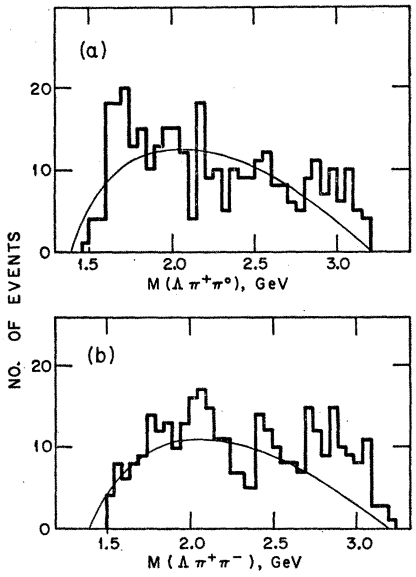

FIG. 23. (a) The $\Lambda\pi^+\pi^0$ mass plot of 344 $\Lambda\pi^+\pi^-\pi^0$ fits at 5.5 GeV/c for which the $\Lambda\pi^+$ or the $\Lambda\pi^0$ mass lie in the region of 1385 MeV after the removal of $\Lambda\pi^+\rho^-$ and $\Lambda\pi^0\rho^0$ events. The events in the overlap region of Fig. 22(c) have only been entered once. The solid curve represents phase space after the removal of $\Lambda\pi^+\rho^-$ and $\Lambda\pi^0\rho^0$ events. (b) The $\Lambda\pi^+\pi^-$ mass plot of 341 $\Lambda\pi^+\pi^-\pi^0$ fits at 5.5 GeV/c for which the $\Lambda\pi^+$ or the $\Lambda\pi^-$ mass lie in the region of 1385 MeV after the removal of $\Lambda\pi^+\rho^-$ and $\Lambda\pi^-\rho^+$ events. The events which simultaneously lie in the 1385 MeV region of the $\Lambda\pi^+$ and $\Lambda\pi^-$ mass have only been entered once. The solid curve represents phase space after the removal of $\Lambda\pi^+\rho^-$ and $\Lambda\pi^-\rho^+$ events.

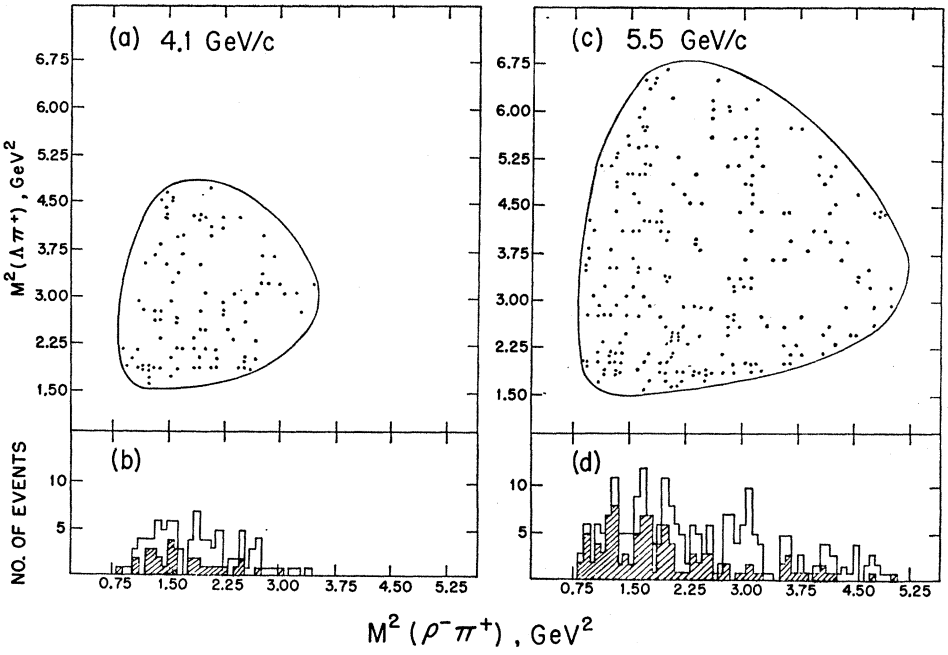

FIG. 24. (a) and (b) are Dalitz plots and $M^2(\rho^-\pi^+)$ projections of events contained in the $\Lambda\pi^+\rho^-$ region of the $\Lambda\pi^+\pi^-\pi^0$ fits at 4.1 GeV/c. The shaded region represents events having $\Delta^2(\rho^-\pi^+)\leq 1.0$ (GeV/c^2). (c) and (d) are the corresponding plots at 5.5 GeV/c.

in the Y^* c.m. system with respect to the normal to the production plane.

The production of $\frac{3}{2}^+$ baryons have been found to be successfully described at lower momenta by this model.[1,22] The same model continues to be a successful description of the $Y_1^{*+}(1385)$ production and decay at the momenta of the present experiment. Figure 32 shows the experimental distributions in $\cos\theta'$ and the Treiman-Yang angle ϕ along with the best fit curves to the distribution $W_{3/2}(\theta,\phi)$.

As for the Λ+meson final states, the production angular distribution for Y^*+meson final states is more sharply peaked than expected from the propagator of the exchanged particle. Figure 33 shows the data for the $Y_1^{*+}(1385)\pi^-$, $Y_1^{*+}(1695)\pi^-$, and $Y_1^{*+}(1385)\rho^-$ final states. The $Y^*\pi$ final states are consistent with $d\sigma/dt\propto\exp(-3|t|)$, similar to the $\Lambda\rho$ and $\Lambda\omega$ final states previously discussed. The $Y^*\rho$ final state may be exhibiting a turnover in the differential cross section near the minimum momentum transfer.

Because of the above observations the absorption model of Jackson *et al.*[23] of $K^*(890)$ exchange with $M1$ dominance was applied to the $Y_1^{*+}(1385)\pi^-$ final state. The starting point of the calculation is the so-called magic formula of Sopkovich[24] which gives the expression for the partial-wave amplitude

$$M_{fi}{}^j=(S_{ff}{}^j)^{1/2}B_{fi}{}^j(S_{ii}{}^j)^{1/2}.$$

Here $B_{fi}{}^j$ is the partial-wave Born amplitude and $S_{ii}{}^j$ and $S_{ff}{}^j$ are the elastic S-matrix elements for the initial and final states, respectively. The exponential decrease of the elastic-scattering angular distribution and imaginary character of the forward-scattering amplitude lead to a single expression for the elastic-scattering S matrix. This is given by

$$S^j=\exp(2i\delta_j)=1-C\exp[-\gamma(j-\tfrac{1}{2})^2]$$

where

$$C=\sigma_t/4\pi A\,,\quad \gamma=1/2q^2A\,.$$

Here σ_t is the total scattering cross section for the initial- (final-) state particles. The parameter A speci-

TABLE XI. Density matrix elements for $Y_1^*(1385)$+vector-meson production.

Final state	Beam momentum (GeV/c)	ρ_{33}	Reρ_{3-1}	Reρ_{31}	ρ_{11}	ρ_{1-1}	Reρ_{10}
$Y_1^{*+}(1385)\rho^-$	4.1	0.31±0.10	0.07±0.10	−0.09±0.10	0.30±0.06	−0.47±0.08	−0.33±0.09
	5.5	0.24±0.06	−0.08±0.05	−0.13±0.06	0.25±0.04	−0.37±0.05	−0.33±0.05
$Y_1^{*0}(1385)\phi$	4.1	0.29±0.22	0.36±0.21	−0.34±0.15	0.24±0.15	0.12±0.20	−0.10±0.21
	5.5	0.07±0.13	−0.04±0.12	−0.02±0.15	0.30±0.08	−0.07±0.12	−0.02±0.12

[22] G. B. Chadwick, D. J. Crennell, W. T. Davies, M. Derrick, J. H. Mulvey, P. B. Jones, D. Radojicic, C. A. Wilkinson, A. Bettini, M. Cresti, S. Limentani, L. Peruzzo, and R. Santangelo, Phys. Letters **6**, 309 (1963); Brandt Kehoe, Phys. Rev. Letters **11**, 93 (1963).
[23] J. D. Jackson, J. T. Donohue, K. Gottfried, R. Keyser, and B. E. Y. Svensson, Phys. Rev. **139**, B428 (1965).
[24] N. J. Sopkovich, Nuovo Cimento **26**, 186 (1962).

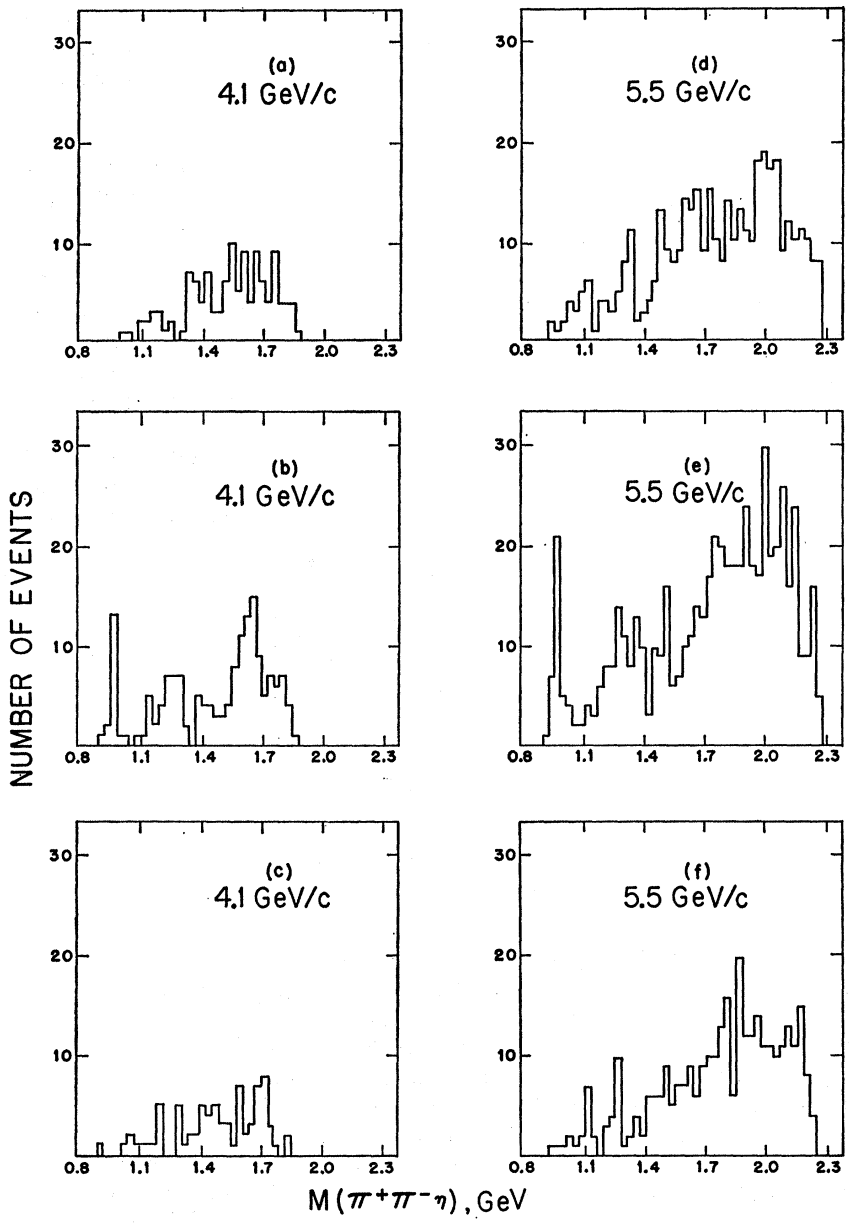

FIG. 25. (a) The $\pi^+\pi^-\eta$ mass for $\Lambda\pi^+\pi^-\eta$ fits at 4.1 GeV/c where the unfitted M^2, defined in $K^-+p\rightarrow\Lambda+\pi^++\pi^-+M$, is required to lie between 0.15 and 0.25 GeV^2. (b) The $\pi^+\pi^-\eta$ mass at 4.1 GeV/c, where the unfitted M^2 is required to lie between 0.25 and 0.36 GeV^2. (c) The $\pi^+\pi^-\eta$ mass at 4.1 GeV/c, where the unfitted M^2 is required to lie between 0.36 and 0.49 GeV^2. (d)–(f) are corresponding plots at 5.5 GeV/c.

fies the elastic-scattering exponential falloff in the form $d\sigma/dt\sim\exp(-A|t|)$, and q is the c.m. momentum of the incident particles. The initial-state parameters may be obtained from the measured total cross sections[25] and elastic angular distributions.[26] We have used $C_i=0.61$ and $\gamma_i=0.039$ at 4.1 GeV/c and $C_i=0.59$ and $\gamma_i=0.027$ at 5.5 GeV/c. The final-state parameters are not known but calculations indicate that the production angular distribution is fairly insensitive to reasonable values of γ_f so that $\gamma_f=\gamma_i$ has been used. Figure 33 shows that the production angular distribution re-

TABLE XII. The $Y_1^*(1385)$+vector-meson density matrix elements compared with the predictions of the independent-quark model.[a]

Final state	Beam momentum (GeV/c)	$\rho_{11}+\rho_{1-1}$	$\frac{4}{5}\rho_{33}+\frac{4}{3}\sqrt{3}\,\mathrm{Re}\rho_{3-1}$
$Y_1^{*+}(1385)\rho^-$	4.1	-0.17 ± 0.10	0.57 ± 0.25
	5.5	-0.12 ± 0.06	0.14 ± 0.15
$Y_1^{*0}(1385)\phi$	4.1	0.36 ± 0.25	$1.2\ \pm0.6$
	5.5	0.23 ± 0.15	$0\ \ \pm0.3$

[a] Reference 27.

[25] W. F. Baker, R. L. Cool, E. W. Jenkins, T. F. Kycia, R. H. Phillips, and A. L. Read, Phys. Rev. **129**, 2285 (1963); A. N. Diddens, E. W. Jenkins, T. F. Kycia, and K. F. Riley, *ibid.* **132**, 2722 (1963).

[26] J. Mott, R. Ammar, R. Davis, W. Kropac, A. Cooper, M. Derrick, T. Fields, L. Hyman, J. Loken, F. Schweingruber, and J. Simpson, Phys. Letters **23**, 171 (1966).

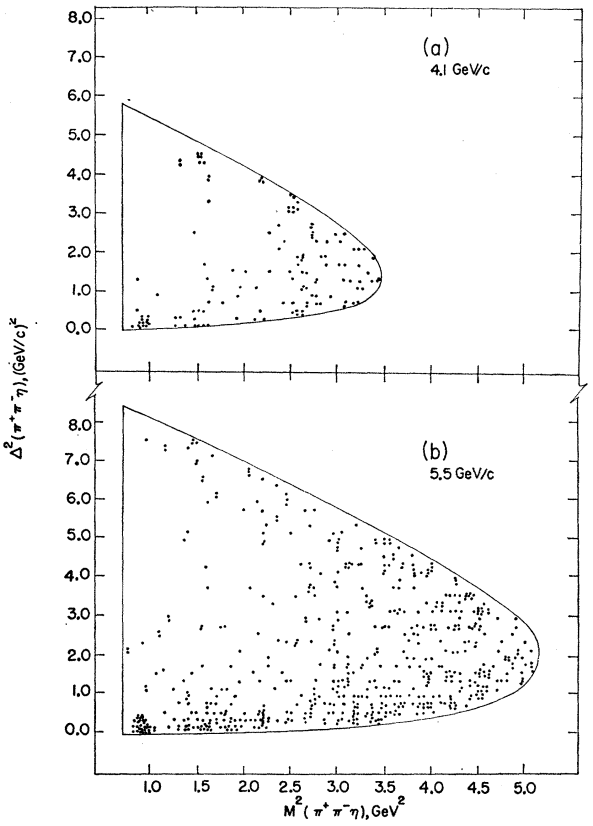

FIG. 26. Chew-Low plots for the $\pi^+\pi^-\eta$ system, where the unfitted M^2, defined in $K^-+p\to\Lambda+\pi^++\pi^-+M$, is required to lie between 0.25 and 0.36 GeV^2. The events have been weighted as described in Sec. II B.

quires the maximum value of $C_f=1$. Using these parameters the effect of the absorption on the density matrix elements is calculated as a function of production angle. Averaging these results over the interval $-1.0\leq\cos\theta\leq-0.5$ in the production angle yields the theoretical values shown in Table X, where results of the analysis described in Sec. IX B, to find the values of ρ_{33}, $\mathrm{Re}\rho_{3\text{-}1}$, and $\mathrm{Re}\rho_{31}$ for the experimental data, are also given. The agreement of the 5.5-GeV/c data with the predictions of the Stodolsky-Sakurai model are seen to be quite good when absorptive effects are taken into account.

In addition to the $Y^*\pi$ final states the density matrix formalism has been applied to the $Y^*\rho$ and $Y^*\phi$ final states and the results are summarized in Table XI. In these cases the decay angular distributions of the baryon and meson resonances are expected to be correlated. In particular the independent-quark model predicts[27] that

$$\rho_{11}+\rho_{1\text{-}1}=\tfrac{4}{3}\sqrt{3}\,\mathrm{Re}\rho_{3\text{-}1}+\tfrac{4}{3}\rho_{33}$$

for $Y_1^*(1385)$+vector-meson production. The data on the $Y^*\rho$ and $Y^*\phi$ final states are summarized in Table XII.

TABLE XIII. Properties of known resonances measured in this experiment.

Particle	Mass (MeV)	Width (MeV)
$Y_1^{*+}(1385)$	1383± 5	31± 6
$Y_1^{*+}(1695)$	1700±20	130±25
f^*	1515±7	35±25
ρ^0	755±15	130±40
X^0	960± 5	

D. Properties of the $Y_1^*(1695)$

In addition to the well-known resonances previously discussed there is clear evidence in the 5.5-GeV/c data for a $\Lambda\pi^+$ enhancement at a mass of ~1700 MeV which we have previously reported[7] and which has since been confirmed by others.[28] This may be seen at $M^2(\Lambda\pi^+)$ ~2.9 GeV^2 in the Dalitz plot of Fig. 3 and more clearly in Fig. 4, which shows the invariant-mass distribution of the $\Lambda\pi^+$ system. Observation of the production angular distributions of Figs. 30 and 33 also indicates that the resonance is produced via a predominantly peripheral mechanism similar to the $Y_1^{*+}(1385)$.

TABLE XIV. $\bar{\sigma}$, the forward hemisphere cross section normalized to $\Lambda\rho^0$ phase space.

Final state	Beam momentum (GeV/c)	Weighted No. of forward events	$\bar{\sigma}$ corrected for other decay modes (μb)[a]
$\Lambda\rho^0$	4.1	21± 7	34±11
	5.5	70±13	14± 3
$\Lambda\omega$	4.1	25± 7	46±12
	5.5	72±11	15± 2
$\Lambda\phi$	4.1	13± 4	48±14
	5.5	33± 8	15± 4
$\Sigma^0\rho^0$	4.1	<4	<8
	5.5	14± 5	3± 1
$\Sigma^0\phi$	4.1	5± 3	21±10
	5.5	6± 4	3± 2
$Y_1^{*0}(1385)\rho^0$	4.1	13±13	29±29
	5.5	30±20	8± 6
$Y_1^{*0}(1385)\phi$	4.1	5± 3	28±16
	5.5	18± 6	11± 4

[a] Reference 13.

The $\Lambda\pi^+$ decay mode establishes that the resonance has unit isospin and a strangeness of -1, while its mass and width are

$$M=1700\pm20\ \mathrm{MeV},$$
$$\Gamma=\ 130\pm25\ \mathrm{MeV}.$$

In addition we find that the $Y_1^*(1695)$ has a negligible

[27] A. Bialas and K. Zelewski, Phys. Letters **26B**, 170 (1968).

[28] D. C. Colley, F. Macdonald, B. Musgrave, W. M. R. Blair, I. S. Hughes, R. M. Turnbull, S. J. Goldsack, K. Paler, L. K. Sisterson, W. Blum, W. W. M. Allison, D. H. Locke, L. Lyons, P. J. Finney, C. M. Fischer, and A. M. Segar, Phys. Letters **24B**, 489 (1967); M. Primer, M. Goldberg, R. Jaeger, V. Barnes, P. Dornan, I. Skillicorn, and Jack Leitner, Phys. Rev. Letters **20**, 610 (1968).

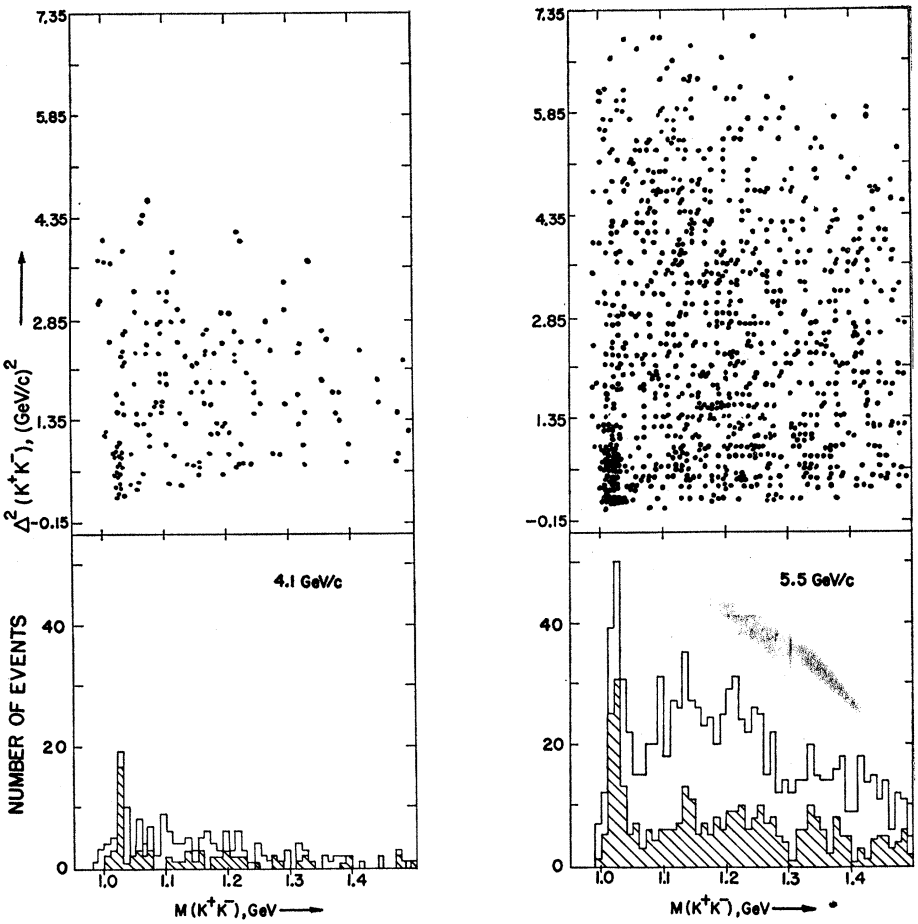

FIG. 27. Chew-Low plots of the K^+K^- system and the K^+K^- mass projections for the $\Lambda K^+K^-\pi^0$ fits. The shaded areas represent events with $\Delta^2(K^+K^-)<1.35$ (GeV/c)^2.

branching ratio for decay into $\Sigma^0\pi^+$, namely,

$$[Y_1^{*+}(1695)\rightarrow\Sigma^0\pi^+]/[Y_1^{*+}(1695)\rightarrow\Lambda\pi^+]<0.2,$$

with a 90% confidence level.

Based on the discussion of Figs. 22 and 23 given in Sec. VI B, we conclude that if the $Y_1^*(1695)$ decays into $Y_1^*(1385)\pi$, then the upper limit on the branching ratio is given by

$$[Y_1^{*+}(1695)\rightarrow Y_1^{*0,+}(1385)\pi^{+,0}]/[Y_1^{*+}(1695)\rightarrow\Lambda\pi^+]<0.5.$$

From an analysis of 452 events satisfying the hypothesis $K^-p\rightarrow\bar{K}^0p\pi^-$ in the same sample of film, one finds little enhancement in the 1700-MeV region of the $\bar{K}^0p$ invariant-mass distribution[5] as may be seen in Fig. 34. This leads to an upper limit for the ratio

$$[Y_1^{*+}(1695)\rightarrow\bar{K}^0p]/[Y_1^{*+}(1695)\rightarrow\Lambda\pi^+]<0.2.$$

The small $\bar{K}N$ coupling indicated by the $\bar{K}^0p$ branching ratio may explain why the $Y_1^*(1695)$ has not been clearly observed in formation experiments.[29]

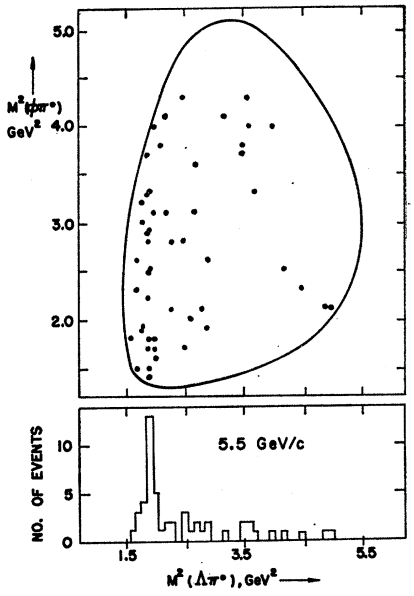

FIG. 28. A Dalitz plot of the $\Lambda\phi\pi^0$ system contained in the $\Lambda K^+K^-\pi^0$ fits at 5.5 GeV/c, with $\Delta^2(K^+K^-)<1.35$ (GeV/c)^2. $\Sigma^0K^+K^-$ fits with $M^2<0$, defined in $K^-+p\rightarrow\Lambda+K^++K^-+M$, have been removed.

[29] R. Armenteros, M. Ferro-Luzzi, D. W. G. Leith, R. Levi-Setti, A. Minten, R. D. Tripp, H. Filthuth, V. Hepp, E. Kluge, H. Schneider, R. Barloutaud, P. Granet, J. Meyer, and J. P. Porte, Phys. Letters 19, 338 (1965).

The formation experiments do, however, show more complexity in this mass region than can be explained by the $Y_1^*(1660)$ and $Y_1^*(1765)$.[30] This may be due to the fact that the $Y_1^*(1695)$ coupling to $\bar{K}N$, although small, is large enough to lead to significant interference effects.

An attempt has been made to determine the spin and parity of the $Y_1^*(1695)$ using a Byers-Fenster analysis.[31] Such a determination is expected to give best results for a sharp resonance having relatively little background. The $Y_1^*(1695)$, however, is a rather

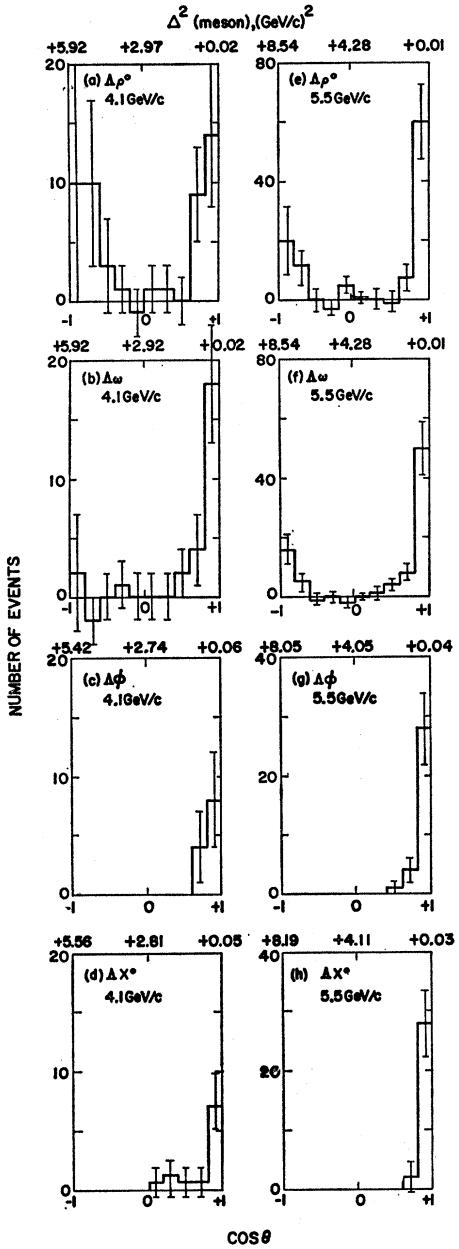

FIG. 29. The production angular distributions of the $\Delta\rho^0$, $\Delta\omega$, $\Delta\phi$, and ΔX^0 events after the subtraction of background. The events have been weighted as described in Sec. II B.

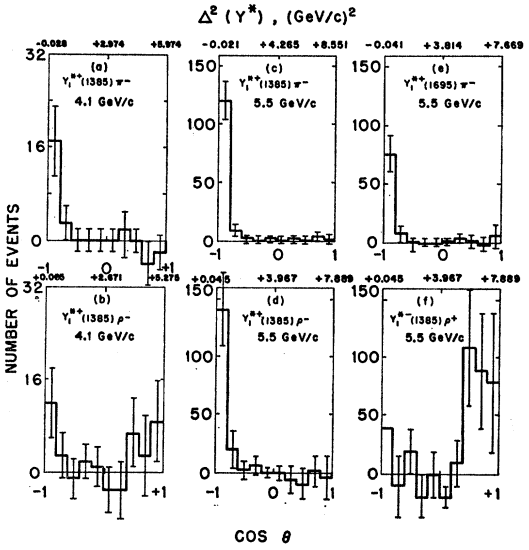

FIG. 30. The production angular distributions, after background subtraction, for the $Y_1^{*+}(1385)\pi^-$ and $Y_1^{*+}(1385)\rho^-$ final states at 4.1 and 5.5 GeV/c and the $Y_1^{*+}(1695)\pi^-$ and $Y_1^{*-}(1385)\rho^+$ final states at 5.5 GeV/c. The events have been weighted as described in Sec. II B.

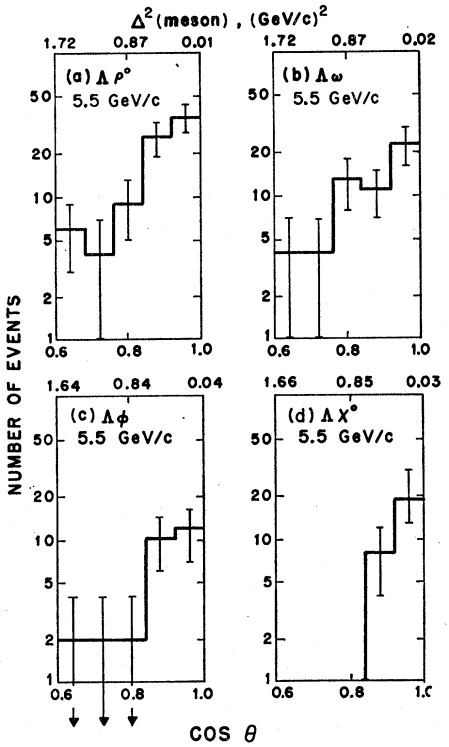

FIG. 31. The production angular distributions in the forward direction, after background subtraction, for the $\Delta\rho^0$, $\Delta\omega$, $\Delta\phi$, and ΔX^0 final states at 5.5 GeV/c. The events have been weighted as described in Sec. II B.

[30] J. Meyer, in *Proceedings of the Heidelberg International Conference on Elementary Particles*, edited by H. Filthuth (North Holland Publishing Company, Amsterdam, 1968), p. 117.

[31] N. Byers and S. Fenster, Phys. Rev. Letters **11**, 52 (1963).

broad resonance with a fair amount of background. In addition the Dalitz plot of Fig. 3 shows possible interference in the region containing the ρ^0 and f. Events resulting from the free decay of $Y_1^*(1695)$ are expected to have a $\pi^+\pi^-$ mass distribution which is symmetric, and this is not the case for the present data. This asymmetry is also evident in the decay angles shown in Fig. 35. For these reasons, and because of limited statistics, no firm conclusions regarding the spin and parity of the $Y_1^*(1695)$ can be drawn from our present data. In particular, we were not able to rule out spin $\frac{1}{2}$.

Finally, we have compared the decay angular distribution of the $Y_1^*(1695)$ with the predictions of the model of Stodolsky and Sakurai[9] as was done in Sec. IX C for the $Y_1^*(1385)$. However, in contrast to the $Y_1^*(1385)$, which is known to be $\frac{3}{2}^+$, the spin and parity of the $Y_1^*(1695)$ are not known and in addition the latter has an asymmetric decay as discussed above. The predicted $W_{3/2^+}(\theta,\phi)$ distribution does not give very good agreement with the data, as one may expect from the distribution shown in Fig. 35.

E. Properties of Other Resonant States

In addition to the $Y_1^*(1695)$, discussed in the previous section, we have also investigated the properties of several other resonant states. Table XIII presents the masses and widths (when measurable) of various states observed with a sufficiently large signal in this experiment. The data for the f^* and X^0 have already been presented elsewhere,[8,17] and have been included in the table for completeness.

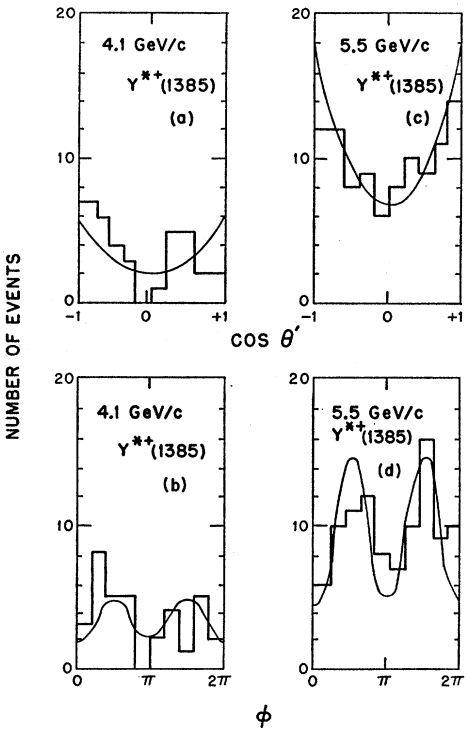

FIG. 32. The $Y_1^{*+}(1385) \to \Lambda\pi^+$ decay angles in the $Y_1^{*+}(1385)$-π^- final state. (a) and (c) are histograms of $\cos\theta'$ at 4.1 and 5.5 GeV/c, where θ' is the Stodolsky-Sakurai angle defined in Sec. IX C. (b) and (d) are histograms of the Treiman-Yang angle ϕ at 4.1 and 5.5 GeV/c. The smooth curves represent the best fit to the data of the distribution $W_{3/2}(\theta,\phi)$ defined in Sec. IX C.

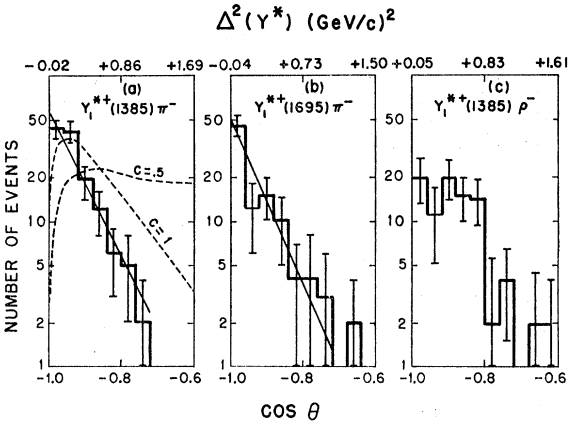

FIG. 33. (a)–(c) are the production angular distributions in the backward direction, after background subtraction, for the $Y_1^{*+}(1385)\pi^-$, $Y_1^{*+}(1695)\pi^-$, and $Y_1^{*+}(1385)\rho^-$ final states, respectively, at 5.5 GeV/c. In (a) the solid curve is a fit to $d\sigma/dt \propto \exp(-a|t|)$, where $a=2.7\pm0.4$ (GeV/c)$^{-2}$, over the range $\Delta^2=-0.02$ to 1.20 (GeV/c)^2. The dashed curves are absorption-model calculations (Ref. 23) for the final-state parameter $C_f=0.5$ and $C_f=1.0$. In (b) the solid curve is a fit to $d\sigma/dt \propto \exp(-a|t|)$, where $a=3.5\pm0.8$ (GeV/c)$^{-2}$, over the range $\Delta^2=-0.04$ to 1.02 (GeV/c)^2.

For the X^0 we have also measured the branching ratio[17]

$$(X^0 \to \rho^0+\gamma)/(X^0 \to \pi+\pi+\eta)=0.31\pm0.15\,,$$

while for the f^* the decay into $K\bar{K}$ was found to be the dominant mode,[8] with no significant evidence for other decay modes.

F. Comparison with Cross-Section Predictions of Various Symmetry Schemes

Because of the forward peripheral nature of the two-body processes observed in this experiment, the observed forward cross sections provide a test of the independent quark model of Alexander, Lipkin, Scheck, and others.[10] Two predictions of this model which can be tested in the experiment, and for which preliminary results have already been presented,[6] are

$$\bar{\sigma}(K^-p \to \Lambda\rho^0)=\bar{\sigma}(K^-p \to \Lambda\omega) \qquad (1)$$

and

$$\bar{\sigma}(K^-p \to \Lambda m^0)=3[\bar{\sigma}(K^-p \to \Sigma^0 m^0) + \bar{\sigma}(K^-p \to Y_1^{*0}(1385)m^0)]. \qquad (2)$$

In these relations, m^0 is any neutral quark-antiquark system and $\bar{\sigma}$ is proportional to the square of the transition matrix element. The quantity $\bar{\sigma}$ was calculated by using only events in the forward hemisphere, correcting for decay modes not seen in this experiment

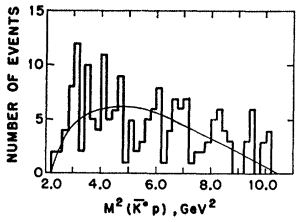

FIG. 34. The square of the $\bar{K}^0p$ mass in the four-constraint $\bar{K}^0p\pi^-$ fits at 5.5 GeV/c after removal of $\bar{K}^*(890)$ and $\bar{K}^*(1400)$ events. The solid curve represents phase space after the removal of the above K^* regions.

and scaling all results to the phase space available to the $\Lambda\rho^0$ final state, using a factor proportional to the final-state c.m. momentum.[32] A comparison of the data with Eq. (2) is limited by the fact that there is information only on the $Y_1^{*0}(1385)\rho^0$ and the $Y_1^{*0}(1385)\phi$ final states. One more relation can be obtained by assuming only K or K^* exchange and provides a connection between the $\Lambda\phi$ and $\Lambda\rho^0$ or $\Lambda\omega$ cross sections, namely,

$$\bar{\sigma}(K^-p\rightarrow\Lambda\phi)=2\bar{\sigma}(K^-p\rightarrow\Lambda\omega). \quad (3)$$

With certain restrictive assumptions, these equations are also derivable from $SU(3)$ or $SU(6)$ symmetries.[33]

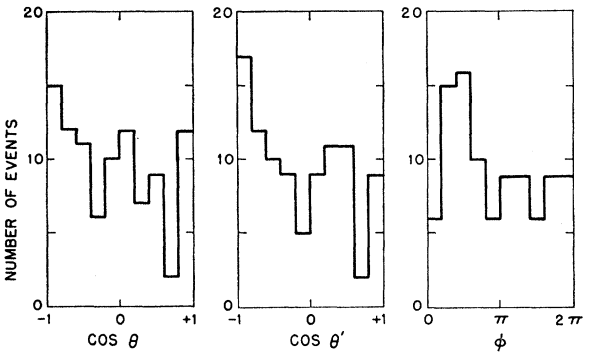

FIG. 35. The decay angular distributions for $Y_1^{*+}(1695)\rightarrow\Lambda\pi^+$ in the $Y_1^{*+}(1695)\pi^-$ final state. The angles θ, θ', and ϕ are analogous to those defined in Sec. IX C for the $Y_1^*(1385)$.

[32] We have not corrected the experimental cross sections by any other factors such as one to compare different reactions at the same Q value, as suggested by S. Meshkov, G. A. Snow, and G. B. Yodh, Phys. Rev. Letters **12**, 87 (1964).

[33] We are informed that there are alternative derivations of Eq. (1) based on $SU(3)$ or universality ideas [P. G. O. Freund, Phys. Rev. Letters **16**, 291 (1966)]; H. J. Lipkin (private communication).

A comparison of the present data with the above predictions may be accomplished by the use of Table XIV, which gives $\bar{\sigma}$ for the reactions of interest. The equality for $\Lambda\rho^0$ and $\Lambda\omega$ predicted by Eq. (1) was found to hold experimentally at both momenta. For the particular cases of the ρ^0 and ϕ mesons, the present experimental results are consistent with Eq. (2). The $\Lambda\phi$ cross sections divided by the values predicted by Eq. (3) are 0.5 ± 0.2 at both 4.1 and 5.5 GeV/c. Further similarities between the $\Lambda\rho^0$ and $\Lambda\omega$ final states can be seen in the density matrix elements given in Table IX. For the $\Lambda\phi$ final state the density matrix elements may be somewhat different from those of the $\Lambda\rho^0$ and $\Lambda\omega$ final states.

Relations analogous to the $\Lambda\rho$, $\Lambda\omega$, and $\Lambda\phi$ cross sections discussed above should hold for the ΛA_2, Λf, and Λf^* cross sections.[34] However, the f^* branching ratios are not well known[13]; also there is recent evidence that the A_2 enhancement may in fact consist of two mass peaks.[35] For these reasons we have not attempted such a comparison with the present data.

ACKNOWLEDGMENTS

We wish to thank our colleagues at the University of Illinois and the University of Wisconsin for their collaboration on the design and construction of the beam transport system, which made this experiment possible. In addition, we are indebted to the personnel of the bubble chamber and ZGS, as well as the scanners, measurers, and programmers at both Argonne and Northwestern for their careful and patient work.

[34] H. J. Lipkin (private communication).

[35] F. Lefebvres, M. N. Focacci, W. Kienzle, C. Lechanoine, B. Levrat, B. Maglić, M. Martin, P. Schübelin, L. Dubal, M. Fischer, P. Grieder, H. A. Neal, and C. Nef, Phys. Letters **19**, 434 (1965); G. Chikovani, B. Levrat, H. R. Blieden, L. Dubal, Maria N. Focacci, D. Freytag, J. Geibel, W. Kienzle, B. C. Maglić, M. Martin, and J. Orear, *ibid.* **25B**, 44 (1967); W. Kienzle, in Proceedings of the Informal Meeting on Experimental Meson Spectroscopy, Philadelphia, 1968 (unpublished); David J. Crennell, Uri Karshon, Kwan Wu Lai, J. Michael Scarr, and Ian O. Skillicorn, Phys. Rev. Letters **20**, 1318 (1968).